

Appendix A

Fundamentals of Piezoelectricity

Abstract The objective of this chapter is to help understand the main concepts and working of piezoelectric sensors and transducers. Accordingly, the chapter presents a simplified explanation of the piezoelectric phenomenon. The chapter begins with a brief overview of some historical milestones, such as the discovery of the piezoelectric effect and the utilization of piezoelectric materials in various applications. Various mechanisms involved in the polarization of dielectric, ferroelectric and piezoelectric materials are discussed. The piezoelectric effect has been explained with basic mathematical formulations based on the intermingling of electric and elastic phenomena. In essence, the chapter describes the basic concept of piezoelectric phenomena that one needs to know while using piezoelectric materials as transducers. For detailed theory on piezoelectric phenomenon, one may refer to standard literature on piezoelectricity (Mason in *Electromechanical Transducers and Wave Filters*, 1942; Mason in *Physical Acoustics and the Properties of Solids*, 1958; Cady in *Piezoelectricity*, 1946; Nalwa in *Ferroelectric Polymers: Chemistry, Physics, and Applications*, 1995; Ikeda in *Fundamentals of Piezoelectricity*, 1996).

Keywords Piezoelectricity · Dielectric · Ferroelectric · Piezoelectric · Piezoelectric effect · PVDF · PVDF-TrFE · Piezoelectric polymers · Smart materials · Sensors · Actuators

A.1 Introduction and Historical Perspective

The name “piezo” derives from the Greek, meaning “to press”; in more modern terminology, we say that the effect intermingles electric and elastic phenomena. Discovered by Curie brothers [6], the piezoelectricity rapidly grew as a new field of research in the last quarter of the nineteenth century. In 1880, Pierre and Jacques Curie found that in certain materials such as zincblende, topaz, and quartz, mechanical stresses were accompanied by macroscopic polarization and hence the production of electric surface charges. The following year, Lippmann [7], from thermodynamic considerations, predicted the converse effect: an imposed voltage produces mechanical deformations or strains the material. The piezoelectric effect remained a curiosity until the early 1920’s when its presence in quartz was utilized to realize crystal resonators for the stabilization of oscillators, thereby launching the field of

frequency control [3]. With the introduction of quartz control, timekeeping moved from the sun and stars to small, man-made sources that exceeded astronomy based references in stability. Since then the advent of the man-made piezoelectric materials widened the field of applications and devices based on piezoelectricity are used in sonar, hydrophone, microphones, piezo-ignition systems, accelerometers and ultrasonic transducers. The discovery of a strong piezoelectric effect in polyvinylidene fluoride (PVDF) polymer, by Kawai in 1969 [8], further added many applications where properties such as mechanical flexibility are desired. Today, piezoelectric applications include smart materials for vibration control, aerospace and astronomical applications of flexible surfaces and structures, sensors for robotic applications, and novel applications for vibration reduction in sports equipment (tennis racquets and snowboards). Recently, the newer and rapidly burgeoning areas of utilization are the non-volatile memory and the integral incorporation of mechanical actuation and sensing microstructures (e.g. POSFET devices) into electronic chips.

A.2 Dielectric, Ferroelectric and Piezoelectric Materials

A.2.1 Electric Polarization

One of the concepts crucial to the understanding of dielectric, ferroelectric and piezoelectric materials is their response to an externally applied electric field. When a solid is placed in an externally applied electric field, the medium adapts to this perturbation by dynamically changing the positions of the nuclei and the electrons. As a result, dipoles are created and the material is said to undergo polarization. The process of dipole formation (or alignment of already existing permanent or induced atomic or molecular dipoles) under the influence of an external electric field that has an electric field strength, E , is called polarization. There are three main types or sources of polarization: electronic, ionic, and dipolar or orientation. A fourth source of polarization is the interfacial space charge that occurs at electrodes and at heterogeneities such as grain boundaries. For an alternating electric field, the degree to which each mechanism contributes to the overall polarization of the material depends on the frequency of the applied field, as shown in Fig. A.1. Each polarization mechanism ceases to function when the applied field frequency exceeds its relaxation frequency.

Electronic polarization may be induced to one degree or another in all atoms. It results from a displacement of the center of the negatively charged electron cloud relative to the positive nucleus of an atom by the electric field, as indicated in the bottom-right of Fig. A.1. This polarization type is found in all dielectric materials, and, of course, exists only while an electric field is present. Ionic polarization occurs only in materials that are ionic. An applied field acts to displace cations in one direction and anions in the opposite direction, which gives rise to a net dipole moment. This phenomenon is illustrated in right-center of Fig. A.1. The third type, orientation polarization, is found only in substances that possess permanent dipole

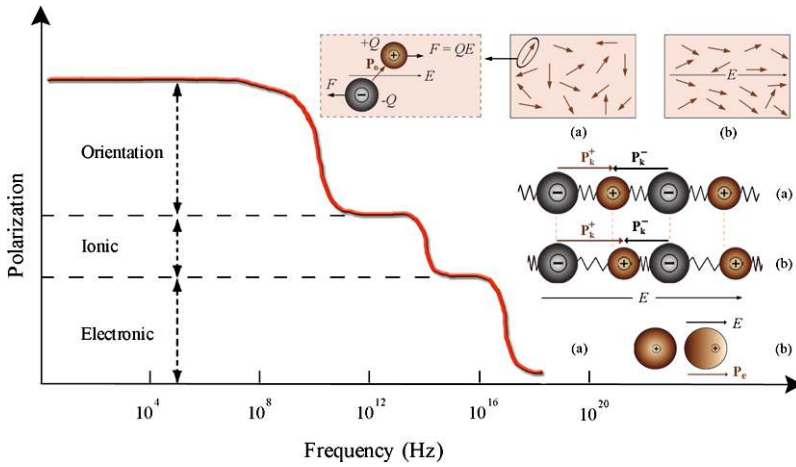


Fig. A.1 Frequency dependence of various polarization mechanisms. The electronic, ionic, and orientation polarization mechanisms are indicated

moments. Polarization results from a rotation of the permanent moments into the direction of the applied field, as represented in top-right of Fig. A.1.

The total electric polarization of a substance is equal to the sum of the electronic, ionic, and orientation (and space-charge) polarizations. It is possible for one or more of these contributions, to the total electric polarization, to be either absent or negligible in magnitude relative to the others. For example, ionic polarization will not exist in covalently bonded materials in which no ions are present. The average polarization per unit volume, \vec{P} , produced by N little electric dipoles (of the electric dipole moment, \vec{p}) which are all aligned, is given by:

$$\vec{P} = \frac{1}{Volume} \sum_{k=0}^N \vec{p}_k \tag{A.1}$$

A.2.2 Dielectric Materials

A dielectric material is one that is electrically insulating (nonmetallic) and exhibits or may be made to exhibit an electric dipole structure; that is, there is a separation of positive and negative electrically charged entities on a molecular or atomic level. The dielectric materials ordinarily exhibit at least one of the polarization types discussed in previous section—depending on the material and also the manner of the external field application. There are two types of dielectrics. The first type is polar dielectrics, which are dielectrics that have permanent electric dipole moments. As depicted in top-right of Fig. A.1, the orientation of polar molecules is random in the absence of an external field. When an external electric field E is present, a torque

is set up and causes the molecules to align with E . However, the alignment is not complete due to random thermal motion. The second type of dielectrics is the non-polar dielectrics, which are dielectrics that do not possess permanent electric dipole moment. Electric dipole moments can be induced by placing the materials in an externally applied electric field. Figure A.1 illustrates the state of non-polar molecules with and without an external field.

Dielectric materials are electrically insulating, yet susceptible to polarization in the presence of an electric field. This polarization phenomenon accounts for the ability of the dielectrics to increase the charge storing capability of capacitors, the efficiency of which is expressed in terms of a dielectric constant.

A.2.3 Ferroelectric Materials

Ferroelectrics are the class of dielectric materials which exhibit spontaneous polarization (polarization associated with a spontaneously formed dipole moment)—that is, polarization in the absence of an electric field. The spontaneous polarization of ferroelectric materials can be switched by applying an electric field; its expression is a typical P–E hysteresis loop similar to that shown in Fig. A.5(a). They undergo a structural phase transition from a high temperature paraelectric into a low-temperature ferroelectric phase at Curie temperature. Ferroelectric materials are the dielectric analogue of ferromagnetic materials, which may display permanent magnetic behavior. There must exist permanent electric dipoles in the ferroelectric materials. Ferroelectrics are a class of the polar piezoelectrics (e.g. polarized PZT, PVDF, and P(VDF-TrFE)) and hence all ferroelectric materials are piezoelectric.

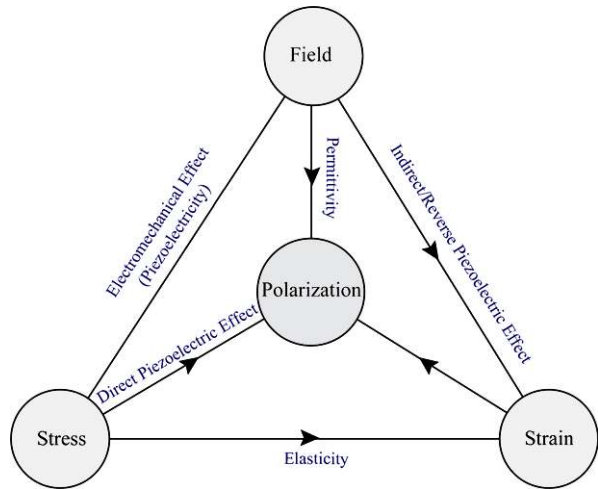
A.2.4 Piezoelectric Materials

Piezoelectrics are the class of dielectric materials which can be polarized, in addition to an electric field, also by application of a mechanical stress (Fig. A.2). This unusual property exhibited by a few dielectric materials is called piezoelectricity, or, literally, pressure electricity. Piezoelectric materials can be divided into polar (which possess a net dipole moment) and non polar piezoelectric materials (whose dipolar moments summed in different directions give a null total moment). A detailed description of the piezoelectric effect is given in following sections.

A.3 The Piezoelectric Effect

The piezoelectric effect, explained with a simple molecular model shown in Fig. A.3, is the generation of an electric charge as a result of a force exerted on

Fig. A.2
Piezoelectricity—An intermingling of electric and elastic phenomena



the material. Before subjecting the material to an external stress the centers of the negative and positive charges of each molecule coincide—resulting into an electrically neutral molecule as indicated in Fig. A.3(a). However, in presence of an external mechanical stress the internal reticular can be deformed, thus causing the separation of the positive and negative centers of the molecule and generating little dipoles as indicated in Fig. A.3(b). As a result, the opposite facing poles inside the material cancel each other and fixed charges appear on the surface. This is illustrated in Fig. A.3(c). That is to say, the material is polarized and the effect called direct piezoelectric effect. This polarization generates an electric field that can be used to transform the mechanical energy, used in the material’s deformation, into electrical energy.

Figure A.4(a) shows the piezoelectric material with two metal electrodes deposited on opposite surfaces. If the electrodes are externally short circuited, with a

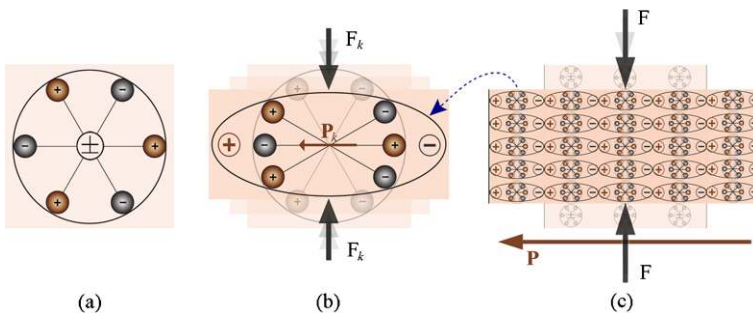


Fig. A.3 Piezoelectric effect explained with a simple molecular model: (a) An unperturbed molecule with no piezoelectric polarization (though prior electric polarization may exist); (b) The molecule subjected to an external force (F_k), resulting in to polarization (P_k) as indicated; (c) The polarizing effect on the surface when piezoelectric material is subjected to an external force

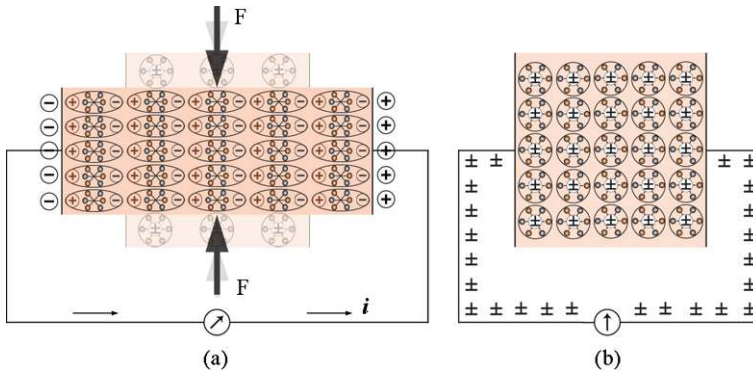


Fig. A.4 Piezoelectric phenomenon: (a) The neutralizing current flow when two terminal of piezo-electric material, subjected to external force, are short circuited; (b) The absence of any current through the short-circuit when material is in an unperturbed state

galvanometer connected to the short circuiting wire, and force is applied the surface of piezoelectric material, a fixed charge density appears on the surfaces of the crystal in contact with the electrodes. This polarization generates an electric field which in turn causes the flow of the free charges existing in the conductor. Depending on their sign, the free charges will move toward the ends where the fixed charges generated by polarization are of opposite sign. This flow of free charge continues until the free charge neutralizes the polarization effect, as indicated in Fig. A.4(a). This implies that no charge flows in the steady state or in the unperturbed state—irrespective of the presence of external force. When the force on the material is removed, the polarization too disappears, the flow of free charges reverses and finally the material comes back to its original standstill state indicated in Fig. A.4(b). This process would be displayed in the galvanometer, which would have marked two opposite sign current peaks. If short-circuiting wire is replaced with a resistance/load, the current would flow through it and hence mechanical energy would be transformed into electrical energy. This scheme is fundamental to various energy harvesting techniques that tap ambient mechanical energy such as vibrations [9] and convert it into usable electrical form.

Some materials also exhibit the reverse piezoelectric effect i.e. a mechanical deformation or strain is produced in the material when a voltage is applied across the electrodes. The strain generated in this way could be used, for example, to displace a coupled mechanical load. This way of transforming the electrical electric energy into usable mechanical energy is fundamental to the applications such as nano-positioning devices.

A.4 Piezoelectric Materials—Static Actions

The piezoelectric materials are anisotropic in nature and hence their electrical, mechanical, and electromechanical properties differ for the electrical/mechanical ex-

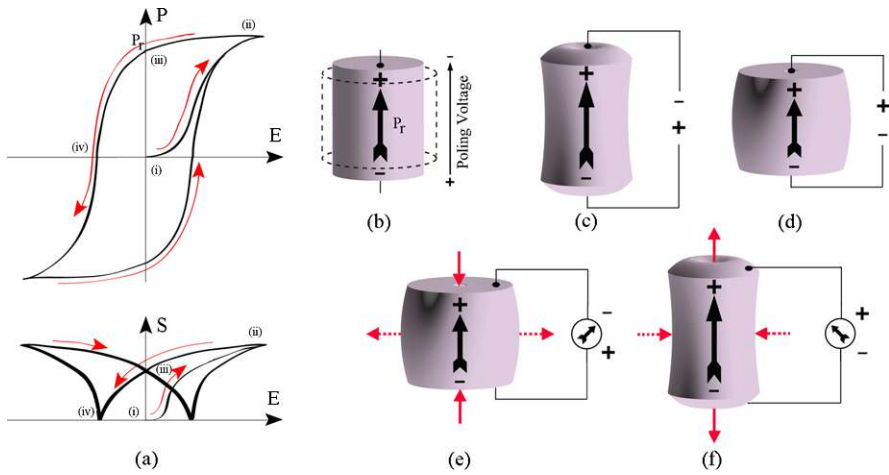


Fig. A.5 Piezoelectric material in sensing and actuating applications. (a) Typical P-E hysteresis plot (top) and the strain versus electric field plot (bottom) of a piezoelectric material. (b) The piezoelectric material before (dotted) and after poling, albeit change in dimension is exaggerated. The polarity of poling voltage is clearly indicated. (c) Material’s dimension when applied voltage has polarity similar to that of poling voltage. (d) Material’s dimension when applied voltage has polarity opposite to that of poling voltage. (e) The generated voltage with polarity similar to poling voltage when compressive force is applied in poling direction. (f) The generated voltage with polarity opposite to poling voltage when tensile force is applied in poling direction

citations along different directions. Using them in various sensing or actuating applications requires a systematic tabulation of their properties—for which, a standardized means for identifying directions is very important. That is to say, once the piezoelectric material is chosen for a particular application, it is important to set the mechanical and electrical axes of operation. Wherever crystals are concerned, the orthogonal axes originally assigned by crystallographers are used for this purpose. A general practice to identify the axes is to assign them the numerals e.g. 1 corresponds to x axis; 2 corresponds to y axis, and 3 corresponds to z axis. These axes are set during “poling”; the process that induces piezoelectric properties in the piezoelectric material. The orientation of the DC poling field determines the orientation of the mechanical and electrical axes. The direction of the poling field is generally identified as one of the axes. The poling field can be applied in such a way that the material exhibits piezoelectric responses in various directions or combination of directions. The poling process permanently changes the dimensions of a piezoelectric material, as illustrated in Fig. A.5(b). The dimension between the poling electrodes increases and the dimensions parallel to the electrodes decrease. In some materials, the poling step is also needed for the introduction of piezoelectric effect. For example, in virgin state the piezoelectric materials such as PVDF, P(VDF-TrFE), and ceramics are isotropic and are not piezoelectric before poling. Once they are polarized, however, they become anisotropic.

After the poling process is complete, a voltage lower than the poling voltage changes the dimensions of the piezoelectric material for as long as the voltage is

applied. A voltage with the same polarity as the poling voltage causes additional expansion along the poling axis and contraction perpendicular to the poling axis, as illustrated in Fig. A.5(c). One can also notice this from the P–E and S–E plots shown in Fig. A.5(a). When a poling field, E , is applied across a piezoelectric material, the polarization as well as the mechanical strain curves follow the path (i)–(ii) on the P–E and S–E plots respectively. When the poling field is removed, the path (ii)–(iii) is followed and piezoelectric material retains certain level of polarization, called remanent polarization, P_r , and experiences permanent strain or permanent change in the dimensions. From operational point of view, the poling procedure shifts the working point from (i) to (iii). After this, whenever a voltage with the same polarity as the poling field is applied, the P–E and S–E plots will follow the curve (iii)–(ii) and hence positive strain will be developed, as indicated in Fig. A.5(a). In other words, there is expansion along the poling axis, as shown in Fig. A.5(c). Similarly, when a voltage with the polarity opposite to the poling voltage is applied the P–E and S–E plots will follow the curve (iii)–(iv), resulting in negative strain. As a result, there is contraction along the poling axis and expansion perpendicular to the poling axis, as indicated in Fig. A.5(d). In both cases, however, the piezoelectric material returns to its poled dimensions on the plots (i.e. working point (iii) on Fig. A.5(a)) when the voltage is removed from the electrodes.

If after completion of the poling process, a compressive and tensile force is applied to the piezoelectric material, a voltage is generated as shown in Fig. A.5(d), (e). With an argument similar to that presented in previous paragraph it can be shown that the generated voltage will have the same polarity as the poling field when a compressive force is applied along the poling axis or a tensile force applied perpendicular to the poling axis. This is illustrated in Fig. A.5(e). Similarly, as indicated in Fig. A.5(f), a voltage with the opposite polarity will result when a tensile force is applied along the poling axis, or when a compressive force is applied perpendicular to the poling axis.

The knowledge of the voltage polarities is very helpful before a piezoelectric material is actually put to use. Generally two or more of the above mentioned actions are present simultaneously. In some cases one type of expansion is accompanied by another type of contraction which compensate each other resulting in no change of volume. For example, the expansion of length of a plate may be compensated by an equal contraction of width or thickness. In some materials, however, the compensating effects are not of equal magnitude and net volume change does occur. In all cases, the deformations are, however, very small when amplification by mechanical resonance is not involved. The maximum displacements are on the order of a few micro-inches.

A.5 Piezoelectric Effect—Basic Mathematical Formulation

This section presents basic mathematical formulation describing the electromechanical properties of piezoelectric materials. The presentation is based on the linear the-

ory of piezoelectricity [10], according to which, piezoelectric materials have a linear profile at low electric fields and at low mechanical stress levels.¹ For the range of mechanical stresses and electrical fields used in this book, the piezoelectric materials exhibit the linear behavior.

As explained in previous sections, when a poled piezoelectric material is mechanically strained it becomes electrically polarized, producing fixed electric charge on the surface of the material. If electrodes are attached to the surfaces of the material, the generated electric charge can be collected and used. Following the linear theory of piezoelectricity [10], the density of generated fixed charge in a piezoelectric material is proportional to the external stress. In a first mathematical formulation, this relationship can be simply written as:

$$P_{pe} = d \times T \quad (\text{A.2})$$

where P_{pe} is the piezoelectric polarization vector, whose magnitude is equal to the fixed charge density produced as a result of piezoelectric effect, d is the piezoelectric strain coefficient and T is the stress to which piezoelectric material is subjected. For simplicity, the polarization, stress, and the strain generated by the piezoelectric effect have been specified with the ‘ pe ’ subscript, while those externally applied do not have any subscript. In a similar manner, the indirect/reverse piezoelectric effect can be formulated as:

$$S_{pe} = d \times E \quad (\text{A.3})$$

where S_{pe} is the mechanical strain produced by reverse piezoelectric effect and E is the magnitude of the applied electric field. Considering the elastic properties of the material, the direct and reverse piezoelectric effects can alternatively be formulated as:

$$P_{pe} = d \times T = d \times c \times S = e \times S \quad (\text{A.4})$$

$$T_{pe} = c \times S_{pe} = c \times d \times E = e \times E \quad (\text{A.5})$$

where c is the elastic constant relating the generated stress and the applied strain ($T = c \times S$), s is the compliance coefficient which relates the deformation produced by the application of a stress ($S = s \times T$), and e is the piezoelectric stress constant.

A.5.1 Contribution to Elastic Constants

The piezoelectric phenomenon causes an increase of the material’s stiffness. To understand this effect, let us suppose that the piezoelectric material is subjected to a

¹At high electric field or high mechanical stress, they may show considerable nonlinearity.

strain S . This strain will have two effects: One, it will generate an elastic stress T_e , proportional to the mechanical strain ($T_e = c \times S$); and two, it will generate a piezoelectric polarization $P_{pe} = e \times S$ according to Eq. (A.4). This polarization will create an internal electric field in the material E_{pe} given by:

$$E_{pe} = \frac{P_{pe}}{\varepsilon} = \frac{e \times S}{\varepsilon} \quad (\text{A.6})$$

where ε is the dielectric constant of the material. Assuming a compressive stress, applied on the piezoelectric material along the poling direction, it is known from Fig. A.5(d) that the resulting electric field of piezoelectric origin will have a direction same as that of poling field. Further, it is also known from Fig. A.5(c) and related discussion in previous section that the presence of an electric field with polarity same as that of poling field results in positive strain and hence the expansion of piezoelectric material in the poling direction. That is say, the electric field (E_{pe} from Eq. (A.6)), of piezoelectric origin, produces a stress which opposes the applied external stress. This is also true if the external applied stress is tensile in nature. The stress $T_{pe} (= e \times E_{pe})$, produced by the electric field E_{pe} , as well as that of elastic origin, is against the material's deformation. Consequently, the stress generated by the strain S is:

$$T = T_e + T_{pe} = c \times S + \frac{e^2}{\varepsilon} \times S = \left(c + \frac{e^2}{\varepsilon} \right) \times S = \bar{c} \times S \quad (\text{A.7})$$

Thus, piezoelectric effect results in an increased elastic constant or in other words, the material gets stiffened in presence of piezoelectric effect. The constant \bar{c} , in Eq. (A.7), is the piezoelectrically stiffened constant.

A.5.2 Contribution to Dielectric Constants

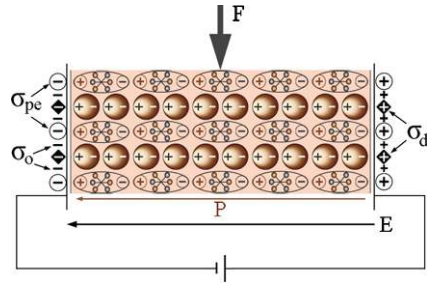
When an external electric field E is applied between two electrodes where a material of dielectric constant ε exists, an electric displacement is created toward those electrodes, generating a surface charge density $\sigma = \sigma_o + \sigma_d$, as shown in Fig. A.6. The magnitude of this electric displacement is $D = \varepsilon \times E$.² If the material is piezoelectric, the electric field E also produces a strain, expressed as $S_{pe} = d \times E$. This strain, of reverse piezoelectric origin, can be positive or negative depending on the direction of the external electric field with respect to the poling field. As discussed

²The free charge density which appears on the electrodes, will be the sum of the charge density which appears in vacuum plus the one that appears induced by the dielectric effect, i.e.:

$$\sigma = \sigma_o + \sigma_d = \varepsilon_o \times E + \chi \times E = (\varepsilon_o + \chi) \times E = \varepsilon \times E \quad (\text{A.8})$$

where ε_o is the vacuum dielectric permittivity and χ is the dielectric susceptibility of the material.

Fig. A.6 Schematic diagram indicating different electrical displacements associated with a piezoelectric and dielectric material



in previous section, if the direction of external field is same as that of poling field, the strain is positive and material undergoes expansion along the direction of poling field. This is illustrated in Fig. A.5(c). It is also evident from Fig. A.5(f) that the expansion of material along poling field (or compression perpendicular to poling field) generates a voltage having polarity opposite to that of poling field or opposite to the external applied field. The situation is similar to the one shown in Fig. A.6. In essence, this means the polarization, and hence the surface charge density, increases when the direction of applied external field is same as that of poling field. In fact, using Fig. A.5(d) and Fig. A.5(e), it can easily be shown that the surface charge density increases even if the direction of applied external field is opposite to that of the poling field. Thus, the strain, of reverse piezoelectric origin, results in polarization and therefore the surface charge density is increased by an amount $P_{pe} = e \times S_{pe} = e \times d \times E$ (Fig. A.6). If the electric field is maintained constant, the additional polarization due to piezoelectric effect increases the electric displacement of free charges toward the electrodes by the same magnitude i.e. $\sigma_{pe} = P_{pe}$. Therefore, the total electrical displacement is:

$$D = \epsilon \times E + P_{pe} = \epsilon \times E + e \times d \times E = \bar{\epsilon} \times E \tag{A.9}$$

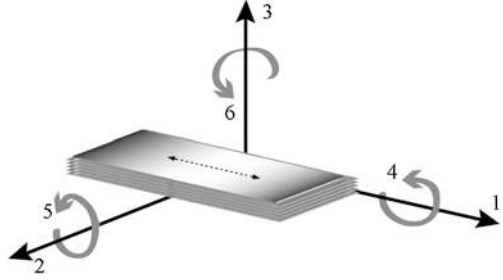
where $\bar{\epsilon}$ is the effective dielectric constant.

A.5.3 Piezoelectric Linear Constitutive Relations

So far, the individual effect of piezoelectricity on the elastic and dielectric has been discussed. In actual practice, piezoelectricity is a cross coupling between the elastic variables, stress T and strain S , and the dielectric variables, electric charge density D and electric field E . This coupling in piezoelectric materials is discussed in this sub-section with help of commonly used linear electro-elastic constitutive equations.

According to the linear theory of piezoelectricity [10], the tensor relation to identify the coupling between mechanical stress, mechanical strain, electric field and electric displacement is given as:

Fig. A.7 Tensor directions for defining the constitutive relations. In PVDF, 1 corresponds to the draw direction (indicated by dotted line), 2 to the transverse direction, and 3 to thickness (also the poling axis)



$$S_p = s_{pq}^E T_q + d_{pk} E_k \quad (\text{A.10})$$

$$D_i = d_{iq} T_q + \varepsilon_{ik}^T E_k \quad (\text{A.11})$$

where, s_{pq}^E is elastic compliance tensor at constant electric field, ε_{ik}^T is dielectric constant tensor under constant stress, d_{kp} is piezoelectric constant tensor, S_p is the mechanical strain in p direction, D_i is electric displacement in i direction, T_q is mechanical stress in q direction, and E_k is the electric field in k direction. The common practice is to label directions as depicted in Fig. A.7. In case of materials such as PVDF, the stretch direction is denoted as “1” and the axis orthogonal to the stretch direction in the plane of the film becomes “2”. The polarization axis (perpendicular to the surface of the film) is denoted as “3”. The shear planes are indicated by the subscripts “4”, “5”, “6” and are perpendicular to the directions “1”, “2”, and “3” respectively. Using these directions, Eqs. (A.1) and (A.2) can be displayed in matrix form as follows:

$$\begin{bmatrix} S_1 \\ S_2 \\ S_3 \\ S_4 \\ S_5 \\ S_6 \end{bmatrix} = \begin{bmatrix} s_{11}^E & s_{12}^E & s_{13}^E & s_{14}^E & s_{15}^E & s_{16}^E \\ s_{21}^E & s_{22}^E & s_{23}^E & s_{24}^E & s_{25}^E & s_{26}^E \\ s_{31}^E & s_{32}^E & s_{33}^E & s_{34}^E & s_{35}^E & s_{36}^E \\ s_{41}^E & s_{42}^E & s_{43}^E & s_{44}^E & s_{45}^E & s_{46}^E \\ s_{51}^E & s_{52}^E & s_{53}^E & s_{54}^E & s_{55}^E & s_{56}^E \\ s_{61}^E & s_{62}^E & s_{63}^E & s_{64}^E & s_{65}^E & s_{66}^E \end{bmatrix} \begin{bmatrix} T_1 \\ T_2 \\ T_3 \\ T_4 \\ T_5 \\ T_6 \end{bmatrix} + \begin{bmatrix} d_{11} & d_{12} & d_{13} \\ d_{21} & d_{22} & d_{23} \\ d_{31} & d_{32} & d_{33} \\ d_{41} & d_{42} & d_{43} \\ d_{51} & d_{52} & d_{53} \\ d_{61} & d_{62} & d_{63} \end{bmatrix} \begin{bmatrix} E_1 \\ E_2 \\ E_3 \end{bmatrix} \quad (\text{A.12})$$

$$\begin{bmatrix} D_1 \\ D_2 \\ D_3 \end{bmatrix} = \begin{bmatrix} d_{11} & d_{12} & d_{13} & d_{14} & d_{15} & d_{16} \\ d_{21} & d_{22} & d_{23} & d_{24} & d_{25} & d_{26} \\ d_{31} & d_{32} & d_{33} & d_{34} & d_{35} & d_{36} \end{bmatrix} \begin{bmatrix} T_1 \\ T_2 \\ T_3 \\ T_4 \\ T_5 \\ T_6 \end{bmatrix} + \begin{bmatrix} \varepsilon_{11}^T & \varepsilon_{12}^T & \varepsilon_{13}^T \\ \varepsilon_{21}^T & \varepsilon_{22}^T & \varepsilon_{23}^T \\ \varepsilon_{31}^T & \varepsilon_{32}^T & \varepsilon_{33}^T \end{bmatrix} \begin{bmatrix} E_1 \\ E_2 \\ E_3 \end{bmatrix} \tag{A.13}$$

Another fundamental parameter used in electromechanical applications is the electromechanical coupling factor k . The electromechanical coupling factor, which measures the ability of a material to interconvert electrical and mechanical energy, is expressed as:

$$k^2 = \frac{\text{Converted Mechanical Energy}}{\text{Input Electrical Energy}} \tag{A.14}$$

or

$$k^2 = \frac{\text{Converted Electrical Energy}}{\text{Input Mechanical Energy}} \tag{A.15}$$

In many cases, processing conditions such as extrusion and the particular crystal symmetry of piezoelectric material determine which components of the dielectric constant, piezoelectric, and elastic compliance tensors are non-zero and unique. For example, for an unstretched and poled piezoelectric P(VDF-TrFE) copolymer, having 2 mm macroscopic symmetry, the matrix form of Eqs. (A.3) and (A.4) can be written as:

$$\begin{bmatrix} S_1 \\ S_2 \\ S_3 \\ S_4 \\ S_5 \\ S_6 \end{bmatrix} = \begin{bmatrix} s_{11}^E & s_{12}^E & s_{13}^E & 0 & 0 & 0 \\ s_{21}^E & s_{22}^E & s_{23}^E & 0 & 0 & 0 \\ s_{31}^E & s_{32}^E & s_{33}^E & 0 & 0 & 0 \\ 0 & 0 & 0 & s_{44}^E & 0 & 0 \\ 0 & 0 & 0 & 0 & s_{55}^E & 0 \\ 0 & 0 & 0 & 0 & 0 & s_{66}^E \end{bmatrix} \begin{bmatrix} T_1 \\ T_2 \\ T_3 \\ T_4 \\ T_5 \\ T_6 \end{bmatrix} + \begin{bmatrix} 0 & 0 & d_{31} \\ 0 & 0 & d_{32} \\ 0 & 0 & d_{33} \\ 0 & d_{24} & 0 \\ d_{15} & 0 & 0 \\ 0 & 0 & 0 \end{bmatrix} \begin{bmatrix} E_1 \\ E_2 \\ E_3 \end{bmatrix} \tag{A.16}$$

Table A.1 Piezoelectric, dielectric, and elastic properties of PVDF [13–15] and P(VDF-TrFE) copolymer with 75/25 mol% [12]

Coefficient/Parameter	PVDF	P(VDF-TrFE) 75/25 ^a	
		Real	Imaginary
d_{31} (pC/N)	21 ^b	10.7	0.18
d_{32} (pC/N)	1.5 ^b	10.1	0.19
d_{33} (pC/N)	-32.5 ^b	-33.5	-0.65
d_{15} (pC/N)	-27 ^b	-36.3	-0.32
d_{24} (pC/N)	-23 ^b	-40.6	-0.35
s_{11}^E (10^{-10} Pa ⁻¹)	3.65 ^c	3.32	0.1
s_{22}^E (10^{-10} Pa ⁻¹)	4.24 ^c	3.34	0.07
s_{33}^E (10^{-10} Pa ⁻¹)	4.72 ^c	3.00	0.07
s_{44}^E (10^{-10} Pa ⁻¹)	–	94.0	2.50
s_{55}^E (10^{-10} Pa ⁻¹)	–	96.3	2.33
s_{66}^E (10^{-10} Pa ⁻¹)	–	14.4	–
s_{12}^E (10^{-10} Pa ⁻¹)	-1.10 ^c	-1.44	–
s_{13}^E (10^{-10} Pa ⁻¹)	-2.09 ^c	-0.89	–
s_{23}^E (10^{-10} Pa ⁻¹)	-1.92 ^c	-0.86	–
$\varepsilon_{11}^T/\varepsilon_0$	6.9 ^d	7.4	0.07
$\varepsilon_{22}^T/\varepsilon_0$	8.6 ^d	7.95	0.09
$\varepsilon_{33}^T/\varepsilon_0$	7.6 ^d	7.9	0.09

^aReference [12]. ^bReference [13]. ^cReference [14]. ^dReference [15]

$$\begin{aligned}
 \begin{bmatrix} D_1 \\ D_2 \\ D_3 \end{bmatrix} &= \begin{bmatrix} 0 & 0 & 0 & 0 & d_{15} & 0 \\ 0 & 0 & 0 & d_{24} & 0 & 0 \\ d_{31} & d_{32} & d_{33} & 0 & 0 & 0 \end{bmatrix} \begin{bmatrix} T_1 \\ T_2 \\ T_3 \\ T_4 \\ T_5 \\ T_6 \end{bmatrix} \\
 &+ \begin{bmatrix} \varepsilon_{11}^T & 0 & 0 \\ 0 & \varepsilon_{22}^T & 0 \\ 0 & 0 & \varepsilon_{33}^T \end{bmatrix} \begin{bmatrix} E_1 \\ E_2 \\ E_3 \end{bmatrix} \quad (\text{A.17})
 \end{aligned}$$

Due to the fact that electromechanical response depends on a number of factors, including polarization conditions, stress/strain rates, temperatures, and hydrostatic pressure, the reported data for the values of various coefficients in the above equations for PVDF and P(VDF-TrFE) copolymer appear to involve certain inconsistencies. Nevertheless, it is possible to identify the typical values such as those listed in Table A.1.

The above tensor relations of Eqs. (A.5) and (A.6) are used to obtain the electromechanical response of a piezoelectric material along the same or other direction as that of stimulus. An as example, the electromechanical response of P(VDF-TrFE) copolymer, when it is used in the thickness mode i.e. both stress and electric field are along the 3-direction, as in Fig. A.7, can be expressed as [11]:

$$S_3 = s_{33}^E T_3 + d_{33} E_3 \quad (\text{A.18})$$

$$D_3 = d_{33} T_3 + \varepsilon_{33}^T E_3 \quad (\text{A.19})$$

The expression for longitudinal electromechanical coupling factor k_{33} , under similar conditions is:

$$k_{33}^2 = \frac{d_{33}^2}{\varepsilon_{33}^T s_{33}^E} \quad (\text{A.20})$$

The constants d_{33} , ε_{33}^T , and s_{33}^E are frequently found in the manufacturer's data. In Eqs. (A.7) and (A.8), T_3 and E_3 are used as independent variables. If, however, D_3 and S_3 are the independent variables the above relations can also be written as:

$$T_3 = c_{33}^D S_3 - h_{33} D_3 \quad (\text{A.21})$$

$$E_3 = -h_{33} S_3 + \beta_{33}^S D_3 = -h_{33} S_3 + \frac{D_3}{\varepsilon_{33}^S} \quad (\text{A.22})$$

The new constants c_{33}^D , h_{33} , and ε_{33}^S are related to d_{33} , ε_{33}^T , and s_{33}^E by following mathematical relations:

$$\varepsilon_{33}^S = \varepsilon_{33}^T - \frac{d_{33}^2}{s_{33}^E} \quad (\text{A.23})$$

$$h_{33} = \frac{d_{33}}{s_{33}^E \varepsilon_{33}^T} \quad (\text{A.24})$$

$$c_{33}^D = h_{33}^2 \varepsilon_{33}^T + \frac{1}{s_{33}^E} \quad (\text{A.25})$$

$$s_{33}^D = (1 - k_{33}^2) s_{33}^E \quad (\text{A.26})$$

Depending on the independent variables chosen to describe the piezoelectric behavior, there can be two more variants of the (A.9) and (A.10), which are not discussed here. For a deeper understanding of piezoelectricity one may refer to standard literature on piezoelectricity [1–5].

References

1. W.P. Mason, *Electromechanical Transducers and Wave Filters* (Van Nostrand, New York, 1942)

2. W.P. Mason, *Physical Acoustics and the Properties of Solids* (Van Nostrand, Princeton, 1958)
3. W.G. Cady, *Piezoelectricity* (McGraw-Hill, New York, 1946)
4. H.S. Nalwa, *Ferroelectric Polymers: Chemistry, Physics, and Applications* (Marcel Dekker, Inc., New York, 1995)
5. T. Ikeda, *Fundamentals of Piezoelectricity* (Oxford University Press, New York, 1996)
6. P. Curie, J. Curie, Développement, par pression, de l'électricité polaire dans les cristaux hémihédres à faces inclinées. C. R. Acad. Sci. **91**, 294–295 (1880)
7. G. Lippmann, Principe de conservation de l'électricité. Ann. Chim. Phys. **24**(5a), 145–178 (1881)
8. H. Kawai, The piezoelectricity of PVDF. Jpn. J. Appl. Phys. **8**, 975–976 (1969)
9. L. Pinna, R.S. Dahiya, M. Valle, G.M. Bo, Analysis of self-powered vibration-based energy scavenging system, in *ISIE 2010: The IEEE International Symposium on Industrial Electronics*, Bari, Italy (2010), pp. 1–6
10. ANSI/IEEE, IEEE standard on piezoelectricity. IEEE Standard 176-1987 (1987)
11. R.S. Dahiya, M. Valle, L. Lorenzelli, SPICE model of lossy piezoelectric polymers. IEEE Trans. Ultrason. Ferroelectr. Freq. Control **56**, 387–396 (2009)
12. H. Wang, Q.M. Zhang, L.E. Cross, A.O. Sykes, Piezoelectric, dielectric, and elastic properties of poly(vinylidene fluoride/trifluoroethylene). J. Appl. Phys. **74**, 3394–3398 (1993)
13. E.L. Nix, I.M. Ward, The measurement of the shear piezoelectric coefficients of polyvinylidene fluoride. Ferroelectrics **67**, 137–141 (1986)
14. V.V. Varadan, Y.R. Roh, V.K. Varadan, R.H. Tancrrell, Measurement of all the elastic and dielectric constants of poled PVDF films, in *Proceedings of 1989 Ultrasonics Symposium*, vol. 2 (1989), pp. 727–730
15. H. Schewe, Piezoelectricity of uniaxially oriented polyvinylidene fluoride, in *Proceedings of 1982 Ultrasonics Symposium* (1982), pp. 519–524

Appendix B

Modeling of Piezoelectric Polymers

Abstract Piezoelectric polymers are used as transducers in many applications, including the tactile sensing presented in this book. It is valuable to use some form of theoretical model to assess, the performance of a transducer; the effects of design changes; electronics modifications etc. Instead of evaluating the transducer and conditioning electronics independently, which may not result in optimized sensor performance, it is advantageous to develop and implement the theoretical model of transducer in such a way that overall sensor (i.e. transducer + conditioning electronics) performance can be optimized. In this context, the ease with which the conditioning electronics can be designed with a SPICE like software tool, makes it important to implement the theoretical model of transducer also with a similar software tool. Moreover, with SPICE it is easier to evaluate the performance of transducer, both, in time and frequency domains. The equivalent model of piezoelectric polymers—that includes the mechanical, electromechanical and dielectric losses—and SPICE implementation of the same are presented in this chapter.

Keywords Piezoelectricity · Piezoelectric effect · PVDF · PVDF-TrFE · Piezoelectric polymers · Smart materials · Sensors · Actuators · Simulation · Modeling · Transmission line model · SPICE · Lossy piezoelectric model

B.1 Introduction

Much work has been published on transducers using piezoelectric ceramics, but a great deal of this work does not apply to the piezoelectric polymers because of their unique electrical and mechanical properties [1]. A number of attempts to model the behavior of piezoelectric materials fail to predict the behavior of piezoelectric polymers because of their lossy and dispersive dielectric properties and higher viscoelastic losses. Starting from the Redwood's transmission line version of Mason's equivalent circuit [2], a SPICE implementation of piezoelectric transducer was reported by Morris et al. [3]. Usage of negative capacitance, $-C_0$ (an unphysical electrical circuit element), by Morris et al. was avoided by Leach with the controlled source technique in an alternative SPICE implementation [4]. The models presented in both these works were verified for piezoceramics operating in the actuating mode i.e. with electrical input and mechanical output. The transducer was assumed to

be lossless, and hence, both these implementations are insufficient for evaluating the performance of transducers with significant losses. Püttmer et al. [5] improved these piezoceramics models by involving a resistor—with value equal to that at fundamental resonance—to represent the acoustic losses in the transmission line, under the assumption that transmission line has low losses. Further, the dielectric and electromechanical losses in the transducer were assumed negligible. These assumptions worked well for piezoceramics, but modeling of lossy polymers like PVDF requires inclusion of all these losses. Keeping these facts in view, the equivalent model of piezoelectric polymers—that includes the mechanical, electromechanical and dielectric losses—was developed [6] and SPICE implementation of the same is presented in this chapter.

Following sections present the theory of the lossy model of piezoelectric polymers; its SPICE implementation and its evaluation vis-a-vis experimental results. Using the model presented in this chapter, many design issues associated with the piezoelectric polymers are also discussed.

B.2 Theory

B.2.1 Piezoelectric Linear Constitutive Relations

According to the linear theory of piezoelectricity [7], the tensor relation between mechanical stress, mechanical strain, electric field and electric displacement is:

$$S_p = s_{pq}^E T_q + d_{kp} E_k \quad (\text{B.1})$$

$$D_i = d_{iq} T_q + \varepsilon_{ik}^T E_k \quad (\text{B.2})$$

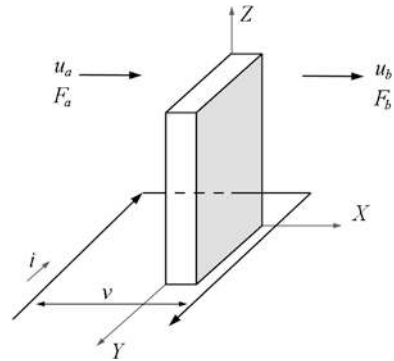
where, S_p is the mechanical strain in p direction, D_i is electric displacement in i direction, T_q is mechanical stress in q direction, E_k is the electric field in k direction, s_{pq}^E is elastic compliance at constant electric field, ε_{ik}^T is dielectric constant under constant stress, and d_{kp} is piezoelectric constant. In the event when polymer is used in the thickness mode, as shown in Fig. B.1, the tensor relations (B.1)–(B.2) can be written as:

$$S_3 = s_{33}^E T_3 + d_{33} E_3 \quad (\text{B.3})$$

$$D_3 = d_{33} T_3 + \varepsilon_{33}^T E_3 \quad (\text{B.4})$$

The constants d_{33} , ε_{33}^T , and s_{33}^E are frequently found in the manufacturer's data for polarized polymers. The analysis is simpler if the variables S_3 , T_3 , D_3 and E_3 are arranged in the alternate way of writing the piezoelectric relation using D_3 and S_3 as independent variables. Thus the equations representing plane compression wave propagation in the x direction (3-direction or the direction of polarization) in a piezoelectric medium are:

Fig. B.1 Piezoelectric polymer operating in thickness mode



$$T_3 = c_{33}^D S_3 - h_{33} D_3 \quad (\text{B.5})$$

$$E_3 = -h_{33} S_3 + \beta_{33}^S D_3 = -h_{33} S_3 + \frac{D_3}{\varepsilon_{33}^S} \quad (\text{B.6})$$

The new constants c_{33}^D , h_{33} and ε_{33}^S are related to the previous constants by:

$$\varepsilon_{33}^S = \varepsilon_{33}^T - \frac{d_{33}^2}{s_{33}^E} \quad (\text{B.7})$$

$$h_{33} = \frac{d_{33}}{s_{33}^E \varepsilon_{33}^T} \quad (\text{B.8})$$

$$c_{33}^D = h_{33}^2 \varepsilon_{33}^T + \frac{1}{s_{33}^E} \quad (\text{B.9})$$

Based on the choice of independent variables, there can be two other variants of the (B.5) and (B.6) which are not given here. Inside polymer, the mechanical strain, mechanical stress and the electrical displacement can be written as:

$$S_3 = \frac{\partial \xi}{\partial x} \quad (\text{B.10})$$

$$\frac{\partial T_3}{\partial x} = \rho \frac{\partial^2 \xi}{\partial t^2} \quad (\text{B.11})$$

$$\text{Div}(D) = 0 \quad (\text{B.12})$$

where ξ is the displacement of the particles inside polymer, ρ is the density of the polymer. Equation (B.11) is basically Newton's law and (B.12) is Gauss's law. Using (B.5) and (B.10)–(B.12), the mechanical behavior of the particles inside polymer can be described as a wave motion which is given by:

$$\frac{\partial^2 \xi}{\partial t^2} = v^2 \frac{\partial^2 \xi}{\partial x^2} \quad (\text{B.13})$$

where, $v = \sqrt{c_{33}^D/\rho}$ is the sound velocity in the polymer and should not be confused with particle velocity ($\partial\xi/\partial t$).

B.2.2 Losses

In general, the piezoelectric polymers possess frequency dependent mechanical, dielectric and electromechanical losses. These losses can be taken into account by replacing elastic, dielectric and piezoelectric constants in (B.1)–(B.13), with their complex values [1, 8]. In other words, the mechanical/viscoelastic, dielectric and electromechanical losses are taken into account by using complex elastic constant, c_{33}^{D*} ; complex dielectric constant, ε_{33}^{S*} and complex electromechanical coupling coefficient, k_t^* respectively. These complex constants can be written as:

$$c_{33}^{D*} = c_r + jc_i = c_{33}^D(1 + j \tan \delta_m) \quad (\text{B.14})$$

$$\varepsilon_{33}^{S*} = \varepsilon_r - j\varepsilon_i = \varepsilon_{33}^S(1 - j \tan \delta_e) \quad (\text{B.15})$$

$$k_t^* = k_{tr} + jk_{ti} = k_t(1 + j \tan \delta_k) \quad (\text{B.16})$$

where, the subscripts r and i stand for real and imaginary terms and $\tan \delta_m$, $\tan \delta_e$, $\tan \delta_k$ are the elastic, dielectric and electromechanical coupling factor loss tangent, respectively. The complex piezoelectric constants viz: d_{33}^* and h_{33}^* , can be obtained from electromechanical coupling constant k_t^* [7].

B.2.3 Polymer Model with Losses

It is assumed that a one-dimensional compression wave is propagating in X direction of thickness-mode piezoelectric transducer, as shown in Fig. B.1. It is also assumed that the electric field E and the electric displacement D are in the X direction. Let u ($= u_a - u_b$) be the net particle velocity, F ($= F_a - F_b$) be the force, and l_x, l_y, l_z are the dimensions of the polymer. Using (B.5)–(B.6) and (B.10)–(B.12), the mathematical relations for the piezoelectric polymer can be written as:

$$\frac{dF}{dx} = -\rho A_x s u \quad (\text{B.17})$$

$$c^* \frac{d\xi}{dx} = -\frac{1}{A_x} F + h^* D \quad (\text{B.18})$$

$$E = -h^* \frac{d\xi}{dx} + \frac{1}{\varepsilon^*} D \quad (\text{B.19})$$

For simplicity, the subscripts have been removed from these expressions. In these equations, s ($= j\omega$) is the Laplace variable and A_x (where $A_x = l_z \times l_y$) is the

cross-sectional area perpendicular to x axis. Complex elastic constant, piezoelectric constant and dielectric constant are represented by c^* , h^* and ε^* respectively. Numerical values of these constants are obtained from the impedance measurements, by using non linear regression technique [9], discussed in next section.

If the current flowing through the external circuit is i , then charge q on the electrodes is i/s and the electric flux density D is equal to $i/(s \times A_x)$. The particle displacement is related to particle velocity by $\xi = u/s$. From (B.12),

$$\frac{dD}{dx} = 0 \Rightarrow \frac{d(i/s)}{dx} = 0 \Rightarrow \frac{d(h^* i/s)}{dx} = 0 \quad (\text{B.20})$$

Using (B.20) in both sides of (B.17)–(B.18), we have:

$$\frac{d}{dx} \left[F - \frac{h^*}{s} i \right] = \rho A_x s u \quad (\text{B.21})$$

$$\frac{du}{dx} = -\frac{s}{A_x c^*} \left[F - \frac{h^*}{s} i \right] \quad (\text{B.22})$$

$$V_{in} = \frac{h^*}{s} [u_1 - u_2] + \frac{1}{C_0^* s} i \quad (\text{B.23})$$

where, V_{in} is the voltage at the electrical terminals of polymer and C_0^* is its lossy capacitance. Equations (B.21)–(B.22) describe the mechanical behavior and (B.23) describe the electromechanical conversion. It can be noted that (B.21)–(B.22) are similar to the standard telegraphist's equations of a lossy electrical transmission line viz:

$$\frac{dV_t}{dx} = -(L_t s + R_t) I_t \quad (\text{B.24})$$

$$\frac{dI_t}{dx} = -(C_t s + G_t) V_t \quad (\text{B.25})$$

where, L_t , R_t , C_t and G_t are the per unit length inductance, resistance, capacitance and conductance of the transmission line. V_t and I_t are the voltage across and current passing through the transmission line. Comparing (B.21)–(B.22) with (B.24)–(B.25), the analogy between these two sets of equations can be observed. Thus, V_t is analogous to $F - (h^*/s) \times i$; L_t is analogous to $\rho \times A_x$; R_t is zero; I_t is analogous to u ; and $s/(A_x \times c^*) = C_t + G_t$. The right hand side of the last expression is a complex quantity due to complex c^* . By substituting $s = j\omega$ and then comparing coefficients on both sides, the expressions of G_t and C_t can be written as:

$$G_t = \frac{c_i \omega}{(c_r^2 + c_i^2) A_x} \quad (\text{B.26})$$

$$C_t = \frac{c_r}{(c_r^2 + c_i^2) A_x} \quad (\text{B.27})$$

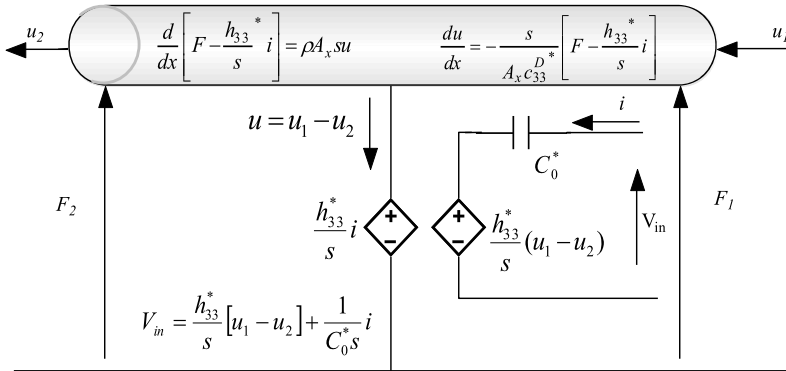


Fig. B.2 Transmission line equivalent model of piezoelectric polymer

Thus, the acoustic transmission can be represented by an analogous lossy electrical transmission line. It is the general practice to represent transmission losses by taking a non-zero R and assuming $G = 0$. But, in acoustics the difference between R and G is not that distinct [10] and it can be shown mathematically that the losses can be represented by any of the following options; (a) Both R and G are used; (b) Only G is used and $R = 0$; (c) Only R is used and $G = 0$. In the analogy presented above, $R = 0$ and $G \neq 0$ and hence the losses in the transmission can be taken into account by having a non-zero value of G . Similarly the electromechanical loss and dielectric loss are considered by using complex values of h and C_0 in (B.23). Complete analogous equivalent circuit for thickness-mode piezoelectric polymer transducer obtained by using (B.21)–(B.23), is shown in Fig. B.2. It should be noted that the model presented here does not include the time-dependence of losses. One may refer [11], for more information on viscoelastic and electromechanical energy losses, over a period of time.

B.3 Measurement of Complex Constants

The dispersive dielectric properties and the internal viscoelastic losses in piezoelectric polymers preclude the convenient use of the classical IEEE standard techniques [7] for determining dielectric and piezoelectric properties. This is due to the fact that the figure of merit, M for piezoelectric polymers is approximately 2–2.5 [1]. As mentioned in the IEEE standard, the parallel frequency, f_p , cannot be measured accurately when $M < 5$. Therefore, one should not apply the IEEE Standard’s equations for k_{33} or k_t assuming that f_p and f_s are the frequencies of maximum and minimum impedance magnitude, respectively.

A technique for characterizing and modeling PVDF was first proposed by Ohigashi [8]. His approach is based on curve fitting the equation for input admittance

Table B.1 Dimensions, densities of the different samples and the electrodes used

Quantity	Symbol	PVDF-TrFE	PVDF-TrFE*	PVDF*	Lead Metaniobate*
Density (kg/m ³)	ρ	1880	1880	1780	6000
Thickness (m)	l_x	50×10^{-6}	0.408×10^{-3}	0.27×10^{-3}	1.55×10^{-3}
Width (m)	l_y	7×10^{-3}	–	–	–
Length (m)	l_z	7×10^{-3}	–	–	–
Diameter (m)	D	–	14×10^{-3}	14×10^{-3}	25.2×10^{-3}
Type of Electrode	–	Al+Cr	Au	Al	Ag
Thickness of Electrode (μm)	t_m	0.08	<0.1	<0.1	<10
Area of sample (m ²)	A_x	49×10^{-6}	154×10^{-6}	154×10^{-6}	498.7×10^{-6}

*From [9]

for an unloaded piezoelectric resonator to actual admittance measurements made over a broad frequency range that includes the fundamental half-wave resonance of the sample. To account for the lossy dispersive dielectric properties, he introduced the dielectric loss factor, $\tan \delta_e$ and to account for the internal viscoelastic losses of PVDF, he introduced the mechanical loss factor, $\tan \delta_m$. Although Ohigashi treated the elastic and dielectric constants as complex, the piezoelectric constant was still considered as real. Several other workers, including Smits [12] and Sherrit et al. [13] have introduced methods to determine the mechanical, dielectric, and piezoelectric loss constants. Smits [12] and Sherrit et al. [13] considered all the material parameters as complex, and the losses are given by the corresponding imaginary parts. A good comparison of various methods used for finding the complex constants is presented by Kwok et al. in [9]. In this work, the material parameters of PVDF, P(VDF-TrFE), PZT/epoxy 1-3 composite, and lead metaniobate are calculated from impedance data by using five methods, namely, the IEEE Std. 176 method, the methods of Smits [12] and Sherrit et al. [13], a software package “PRAP” [14], and the nonlinear regression method of authors. Kwok et al. [9] also observed that the for high loss materials like PVDF, the IEEE standard method gives much higher value of k_{33} or k_t , as compared to other methods.

The software package PRAP, which combines the methods of Smits [12] and Sherrit et al. [13], is a simple way of measuring or generating complex coefficients, if the geometry of the sample is known. In this work, PRAP is used to obtain various complex constants from the impedance and phase measurement of one of the P(VDF-TrFE) samples. The dimension, density, type and thickness of metal electrodes on the sample are given in Table B.1 and various complex constants obtained by PRAP analysis are given in Table B.2. For other samples in Tables B.1 and B.2, the data has been taken from [9]. This data was obtained with non linear regression technique, presented in [9].

Table B.2 Material constants of PVDF-TRFE, PVDF and lead metaniobate

Constant		PVDF-TrFE	PVDF-TrFE*	PVDF*	Lead Metaniobate*
k_t	Real	0.202	0.262	0.127	0.334
	Imaginary	-0.0349	0.0037	0.0055	0.0003
c_{33}^{D*} (N/m ²)	Real	1.088×10^{10}	10.1×10^9	8.7×10^9	65.8×10^9
	Imaginary	5.75×10^8	5.15×10^8	1.018×10^9	4.14×10^9
ϵ_{33}^S *	Real	4.64×10^{-11}	38.78×10^{-12}	55.78×10^{-12}	22.84×10^{-10}
	Imaginary	8.45×10^{-12}	4.11×10^{-12}	15.618×10^{-12}	2.033×10^{-11}
h_{33}^* (V/m)	Real	3.03×10^9	4.20×10^9	1.52×10^9	1.79×10^9
	Imaginary	-7.25×10^8	3.90×10^8	3.69×10^8	6.58×10^7
Q		18.78	19.60	8.54	15.87

*From [9]

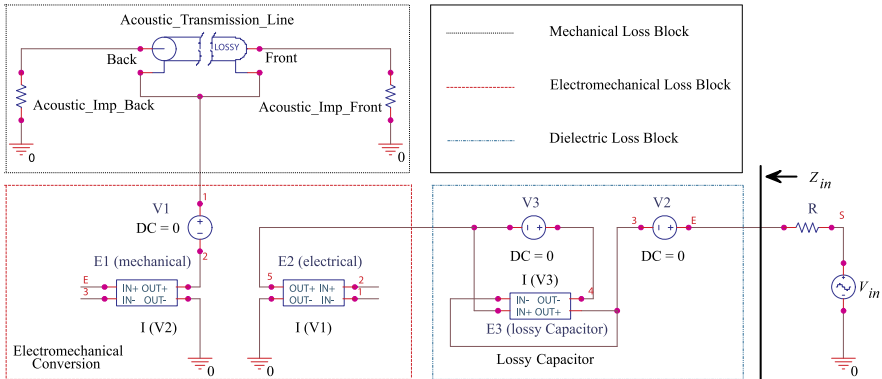


Fig. B.3 Schematic of the equivalent model of piezoelectric polymer implemented with PSpice. The model has been divided into various blocks showing the mechanical/acoustic/viscoelastic, electromechanical/piezoelectric and electric/dielectric losses

B.4 SPICE Implementation

Following the discussion above, the piezoelectric polymer model has been implemented in PSPICE circuit simulator, which is commercially available from ORCAD. Figure B.3 shows the SPICE schematic of the equivalent circuit of Fig. B.2. The mechanical, electromechanical and electrical loss blocks are clearly marked in Fig. B.3. The SPICE implementation of various blocks is explained below. The netlist for SPICE implementation is given at the end of this Appendix.

B.4.1 Mechanical Loss Block

The analogy between (B.21)–(B.22) and (B.24)–(B.25) allows the implementation of mechanical/viscoelastic behavior during acoustic transmission in polymer with a lossy transmission line, which is available in the PSPICE. It can also be implemented with lumped ladder arrangement of G_t , C_t , L_t , R_t . But, here the lossy transmission line is preferred due to the advantages—in terms of accuracy and computation time—offered by the distributed values of G_t , C_t , L_t , R_t , used in it. Further, the lossy transmission line in PSPICE allows the use of frequency dependent expression for G_t , which is desired according to (B.26). The frequency term in G_t is implemented in SPICE, by using the expression $SQRT(-s \times s)$, where, $s (= j\omega)$ is the Laplace operator. The parameters of transmission line viz: G_t , C_t and L_t are obtained by using complex elastic constant i.e. c^* in the analogous expression obtained from the analogy between acoustic wave propagation and the lossy electrical transmission line. For various sample parameters in Tables B.1 and B.2, the transmission line parameters are given in Table B.2. While G_t and C_t are obtained from (B.26)–(B.27); L_t is given by $\rho \times A_x$ and the length, l_x , of the transmission line is equal to the thickness of the sample. As shown in Fig. B.3, the lossy transmission line is terminated into the acoustic impedance of the mediums on two sides of the polymer—which is given by, $Z_m = \rho_m \times v_m \times A_x$. In this expression, ρ_m is the density of medium, v_m is the velocity of sound in medium and A_x is the area of sample. In this work air is present on both sides of samples, hence using, $\rho_m = 1.184 \text{ kg/m}^3$, $v_m = 346 \text{ m/s}$ and A_x from Table B.1, the acoustic impedances of front and backside are given in Table B.3. In a multilayer transducer, the acoustic impedances on both sides can be replaced by transmission lines having parameters (acoustic impedance and time delay etc.) corresponding to the mediums on each side.

B.4.2 Electromechanical Loss Block

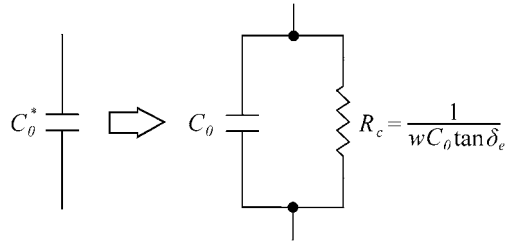
The electromechanical conversion is analogous to the transformer action. It is implemented with the behavioral modeling of controlled sources, i.e. with the ‘ELAPLACE’ function in PSPICE. The currents passing through the controlled sources $E1(\text{mechanical})$ and $E2(\text{electrical})$; are h^*/s times the currents passing through $V2$ and $V1$ respectively. The gain term i.e. ‘ h^*/s ’ used in the controlled sources $E1(\text{mechanical})$ and $E2(\text{electrical})$ —of PSPICE schematic in Fig. B.3—are given in Table B.2. In SPICE, the current in any branch can be measured by using a zero value DC voltage source in that branch. The voltage sources $V1$ and $V2$, shown in Fig. B.3, have zero DC values and are thus used to measure the current passing through them. The complex piezoelectric constant, h^* ensures the inclusion of piezoelectric losses in the model. The complex number operator ‘ j ’ in the expression of h^* is implemented in PSPICE by using the expression $-s/abs(s)$.

Table B.3 Value/expression of parameters used in the SPICE equivalent model

Parameter	PVDF-TiFE	PVDF-TiFE*	PVDF*	Lead Metaniobate*
L_I (H)	0.0921	0.2894	0.274	2.993
G_I	$9.8958 \times 10^{-8} \times \sqrt{(-s \times s)}$	$3.271 \times 10^{-8} \times \sqrt{(-s \times s)}$	$8.61 \times 10^{-8} \times \sqrt{(-s \times s)}$	$1.912 \times 10^{-9} \times \sqrt{(-s \times s)}$
C_I (F)	1.8705×10^{-6}	6.415×10^{-7}	7.39×10^{-7}	3.035×10^{-8}
L_x (m)	50×10^{-6}	0.408×10^{-3}	0.27×10^{-3}	1.55×10^{-3}
Z_m (Ω)	0.020	0.063	0.063	0.204
C_0 (F)	4.545×10^{-11}	14.63×10^{-12}	31.81×10^{-12}	735.05×10^{-12}
h^* /s	$(3.03 \times 10^9 - j7.25 \times 10^8)/s$	$(4.2 \times 10^9 + j3.9 \times 10^8)/s$	$(1.52 \times 10^9 + j3.69 \times 10^8)/s$	$(1.79 \times 10^9 + j6.58 \times 10^7)/s$
Gain of E_3	$1/(s \times (4.54 \times 10^{-11} + j8.28 \times 10^{-12}))$	$1/(s \times (14.63 \times 10^{-12} + j1.55 \times 10^{-12}))$	$1/(s \times (31.81 \times 10^{-12} + j8.91 \times 10^{-12}))$	$1/(s \times (735 \times 10^{-12} + j6.54 \times 10^{-12}))$

*From [9]

Fig. B.4 Equivalent representation of lossy capacitor



B.4.3 Dielectric Loss Block

This block consists of the lossy capacitance of polymer connected to the external voltage source or load. The use of complex permittivity i.e. ε^* , ensures the inclusion of dielectric losses. The lossy capacitor obtained by using ε^* , is equivalent to a lossless capacitor, $C_0 = \varepsilon A_x / l_x$ connected in parallel with the frequency dependent resistor $R_0 = 1 / (\omega C_0 \tan \delta_e)$ as shown in Fig. B.4, where, C_0 is the static lossless capacitance of polymer. The voltage across the equivalent lossy capacitor is given as:

$$V_c = \frac{I_c}{sC_0 + \omega C_0 \tan \delta_e} \quad (\text{B.28})$$

The SPICE circuit simulators allow only constant values of resistors and capacitors. To implement the lossy capacitor—which has the frequency dependent resistor—the behavior modeling of controlled voltage source is used here. The controlled source *E3(lossy capacitor)* is implemented with the ‘ELAPLACE’ function of PSPICE. As per (B.28), the voltage across *E3(lossy capacitor)*, is proportional to the current flowing through itself and measured by the zero value DC source *V3*, as shown in Fig. B.3.

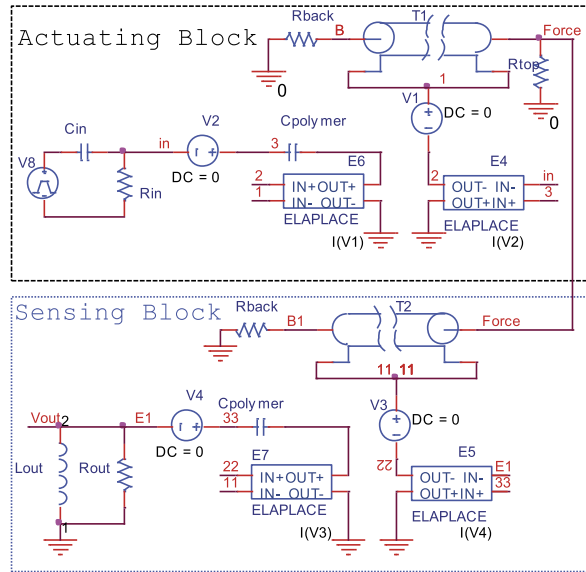
The expressions of the gain terms used in the controlled source *E3(lossy capacitor)*, are given in Table B.3. Again, ω is implemented with the expression $SQRT(-s \times s)$. The netlist for the SPICE implementation shown in Fig. B.3—generated with PSPICE—is given at the end of Appendix B.

B.5 Experiment Versus Simulation

B.5.1 Evaluation of Lossless Model

Since it is difficult to apply forces over wide range of frequencies (\sim MHz) by any mechanical arrangement, the piezoelectric polymer model in sensing mode was evaluated by using the same SPICE model of the polymer in actuating mode. The arrangement, as shown in Fig. B.5, is similar to the standard pulse-echo method, explained in [7]. The actuating mode component of the whole arrangement produces the force needed as the input in sensing component of the SPICE model of

Fig. B.5 SPICE implementation of the standard Pulse-echo method for evaluating the SPICE model of piezoelectric polymer



piezoelectric polymer. The performance of polymer model in sensing mode was evaluated by comparing the simulated response with experiment results reported in [15]. For the purpose of comparison only, the electrical impulse input to the transmitting stage; the load at the output terminal of sensing stage; and various constants were kept same as that used in [15]. The input to the actuating stage is a voltage impulse (300 V, fall time 100 ns) generated by $R_{in} = 100 \Omega$ and $C_{in} = 2$ nF. The output of the sensing stage is terminated in to a load, comprising of a resistance ($R_{out} = 100 \Omega$) and inductance ($L_{out} = 4.7 \mu\text{H}$)—connected in parallel. The losses could not be considered in this comparative study as the constants used in [15] are real numbers. Figure B.6 shows that the simulated outputs of the polymer, both in sensing and actuating mode, are in good agreement with the experiment results, presented in [15].

B.5.2 Evaluation of Lossy Model

The SPICE model presented in earlier section has been evaluated by comparing the simulated impedance and phase plots with the corresponding plots obtained from the measured data of PVDF, P(VDF-TrFE) and lead metaniobate. As mentioned earlier, the approximate lossy models developed for piezoceramic transducers are insufficient for evaluating the behavior of piezoelectric polymers. Keeping this in view, a comparison has also been made with the impedance and phase plots obtained by Püttmer's approach for lossy piezoceramics [5]. Using the PSPICE schematic of Fig. B.3, the simulated impedance, Z_{in} , for all the samples is obtained by dividing

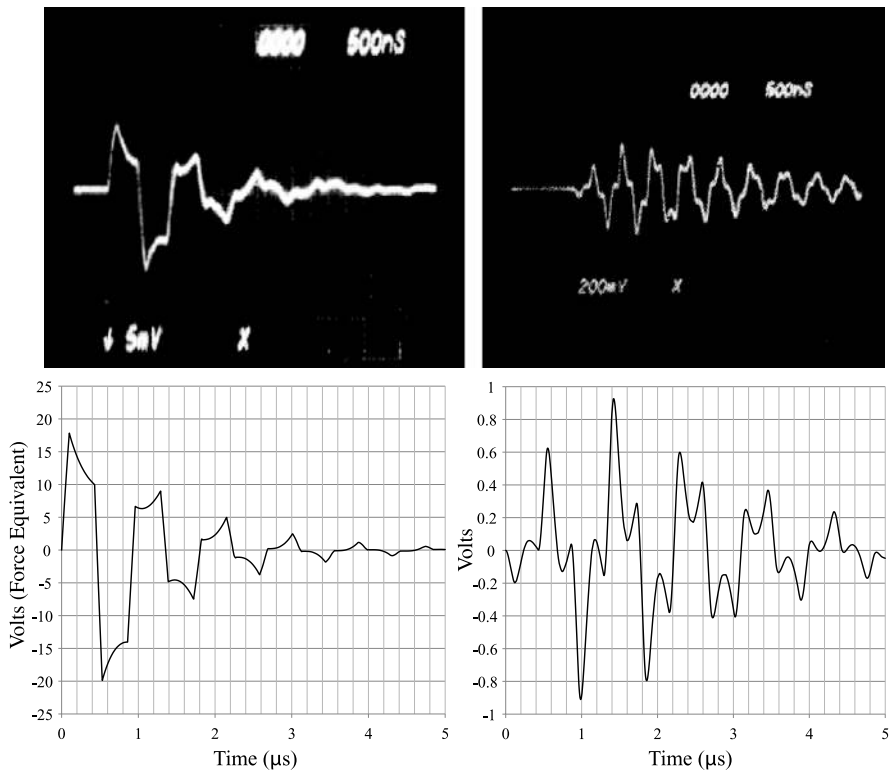


Fig. B.6 (top-left) Force generated by piezoelectric material (actuating component) in the pulse-echo arrangement, reproduced from [15]; (top-right) Voltage output of piezoelectric material (sensing component) in the pulse-echo arrangement, reproduced from [15]; (bottom-left) Simulated force obtained from SPICE model of piezoelectric material (actuating component) (bottom-right) Simulated voltage obtained from SPICE model of piezoelectric material (sensing component)

the voltage at node E (Fig. B.3) with the current passing through this node. For these simulations, the transmission line was terminated into the acoustic impedance of air on both sides and the effect of electrodes present on both sides of polymer was assumed to be negligible due to their negligible small thickness in comparison to that of test samples.

In the case of 50 μm thick P(VDF-TrFE) polymer film, the impedance and phase measurements were obtained with HP4285 LCR meter. The measured impedance and phase plots for other samples, viz: PVDF, P(VDF-TrFE) (0.408 mm thick) and lead metaniobate, used here, are same as those used in [9]. The physical dimensions, calculated complex constants and various parameters of SPICE model for all these samples are given in Tables B.1–B.2.

The impedance and phase plots of lead metaniobate sample, obtained by the SPICE model presented in this work has been compared in Fig. B.7 with those obtained by Püttmer’s approach [5] and measured data. The lead metaniobate sam-

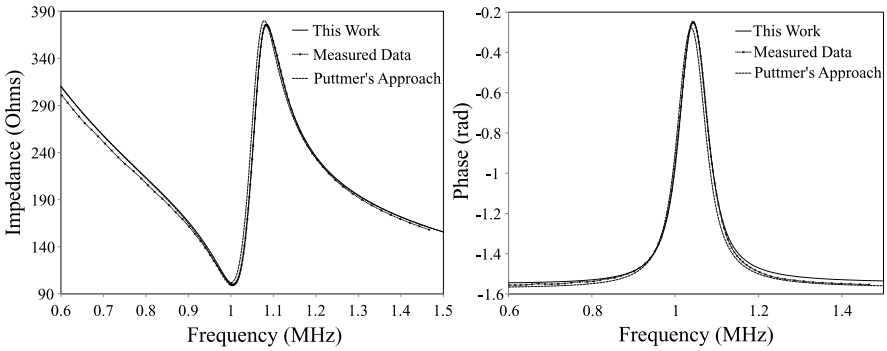


Fig. B.7 Comparison of Impedance (*left*) and Phase (*right*) plots of lead metaniobate sample, with the corresponding plots obtained by the Püttmer’s approach and from the measured impedance data of [9]

ple is chosen here because the model in [5], was evaluated for lead metaniobate. The netlist of the SPICE model using Püttmer’s approach is given in Appendix B. Püttmer’s approach considers the losses in the transmission line only and dielectric and piezoelectric losses are assumed to be negligible. Other difference between Püttmer’s approach and the work presented here is the use of R_t and G_t respectively, to represent the losses in the transmission line. In Püttmer’s approach, L_t is given by $\rho \times A_x$; C_t is given by $1/(c_r \times A_x)$ and a simplified expression of R_t was obtained by assuming the transmission line to be having low loss. The value of R_t was given by $(L_t/Q) \times SQRT(-s \times s)$, where Q is the mechanical quality factor obtained by dividing real part of elastic constant with its imaginary part. It can be observed from Fig. B.7, that the impedance and phase plots of piezoceramics—obtained with the SPICE model presented in this work—are in good agreement with the measured plots and the plots obtained Püttmer’s approach presented in [5]. The agreement between these plots is in line with the observations on the equivalence of using R_t or G_t to represent losses in the acoustic transmission [10].

The impedance and phase plots of two different P(VDF-TrFE) samples, obtained by the SPICE model presented in this work has been compared in Fig. B.8 and Fig. B.9 with those obtained by Püttmer’s approach [5] and from the measured data. The plots in Fig. B.8 correspond to the thin 50 μm film and those in Fig. B.9 correspond to that of 0.408 mm thick film.

An additional plot obtained by considering the transmission losses only, in the SPICE model presented in this work, is also shown in Fig. B.8. It can be observed that the plots obtained with the approach presented here are in good agreement with the measured data. The difference between the approach presented here and that of Püttmer’s approach is more evident in case of thinner polymer film (Fig. B.8) and more so in case of phase plots of both samples. Thus, in case of polymers, Püttmer’s approach leads to a significant deviation from the measured plots.

The comparison of the impedance and phase plots for PVDF is given in Fig. B.10. In case of PVDF, it can be observed that—although an improvement over past

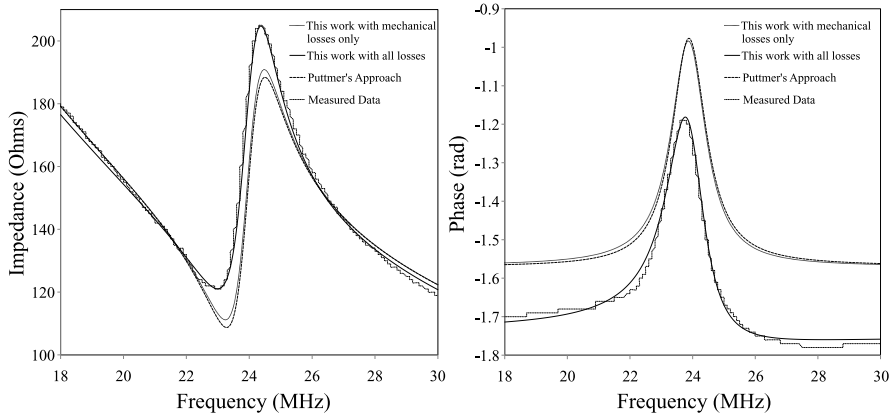


Fig. B.8 Comparison of Impedance (*left*) and Phase (*right*) plots of 50 μm thick PVDF-TrFE polymer film with the corresponding plots obtained by the Püttmer’s approach and from the measured impedance data. The plots obtained by taking the transmission loss only in the SPICE model presented here, has also been shown. In principle, taking only transmission loss only in the model presented here is same as that of Püttmer’s work

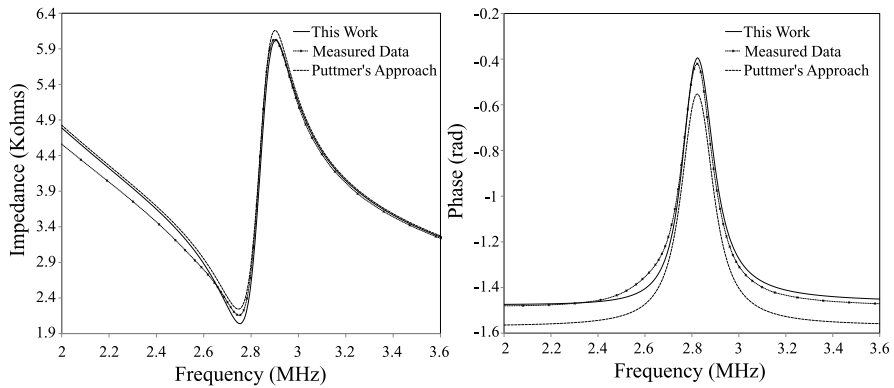


Fig. B.9 Comparison of Impedance (*left*) and Phase (*right*) plots of 0.408 mm thick PVDF-TrFE film with the corresponding plots obtained by the Püttmer’s approach and from the measured impedance data of [9]

approach—the plots obtained with the approach presented in this work still have some discrepancies with the plots obtained from the measured data. The discrepancies are especially higher in the region outside resonance. This can be attributed to the frequency dependence of material parameters [9], which were assumed to be independent of frequency for these simulations. For a piezoelectric transducer the

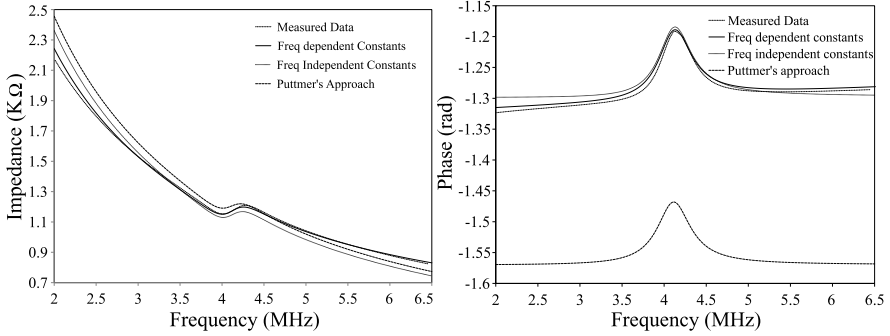


Fig. B.10 Comparison of Impedance (*left*) and Phase (*right*) plots PVDF film with the corresponding plots obtained by the Püttmer's approach and from the measured impedance data of [9]. The plots obtained by using first order frequency dependence of ϵ_{33}^S and $\tan \delta_e$ are also shown

electrical impedance at thickness extensional resonance is given by:

$$Z(f) = \frac{l_x}{i2\pi f \epsilon_{33}^{S*} A_x} \left[1 - k_t^{2*} \frac{\tan(\pi f l_x \sqrt{\rho/c_{33}^{D*}})}{\pi f l_x \sqrt{\rho/c_{33}^{D*}}} \right] \quad (\text{B.29})$$

where, f is the frequency. It can be noticed from (B.29) that outside resonance the impedance depends on ϵ_{33}^{S*} and hence on the ϵ_{33}^S and $\tan \delta_e$ and hence as a first approximation, taking into account the frequency dependence of ϵ_{33}^S and $\tan \delta_e$ should improve the simulation results. Following Kwok's approach, presented in [9], we obtained values of ϵ_{33}^S and $\tan \delta_e$ at various frequencies of the measured impedance data. It was observed that these constants vary with frequency. Considering the data values of ϵ_{33}^S and $\tan \delta_e$ at frequencies outside resonance, a first order frequency dependence of ϵ_{33}^S and $\tan \delta_e$ was obtained by linear fit of the ϵ_{33}^S and $\tan \delta_e$ versus frequency plots. Using these frequency dependent constants in the SPICE model, the impedance and phase plots were obtained. As shown in Fig. B.10, this improves the match between the simulated plots and plots from the measured data. The matching can be further improved—albeit, at the cost of computation power—by using a higher order frequency dependence of ϵ_{33}^S and $\tan \delta_e$ and also the frequency dependence of other material constants viz: c_{33}^{D*} and k_t^* .

B.6 Relative Contribution of Various Losses

Having presented the model with all the losses, the next question that comes to mind is—what is their relative contribution? If the contribution of a particular loss component far outweighs others, then such an argument can be a basis for using a simplified model. To evaluate the role of various loss components, the SPICE model was used to simulate impedance and phase under various combinations of losses. Impedance

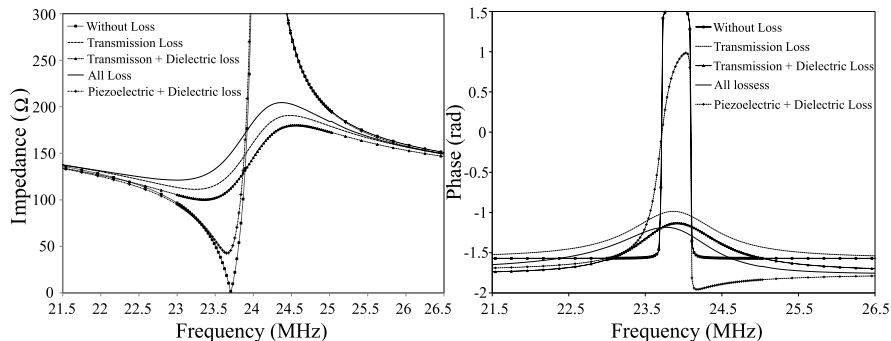


Fig. B.11 Impedance (*left*) and Phase (*right*) plots comparing the relative contribution of various losses. Simulations were performed under assumption of different combinations of losses

and phase plots so obtained are shown in Fig. B.11. It can be noticed that inclusion of only acoustic/transmission losses gives a first approximation of the impedance and phase, which is further improved by the dielectric and piezoelectric losses.

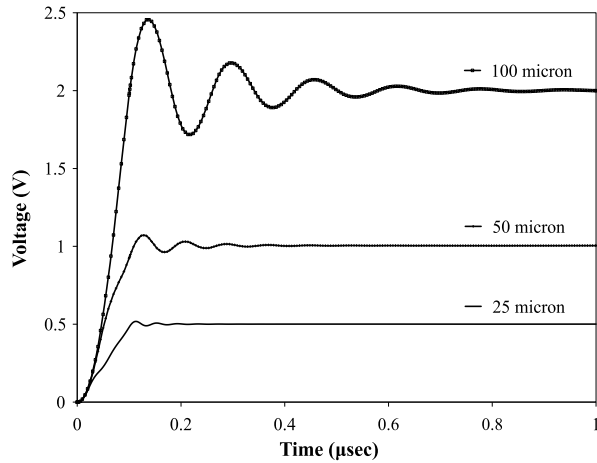
B.7 Design Issues Associated with Piezoelectric Polymer Film

The model developed for piezoelectric polymers can be used to study the effect of various parameters used in the model, which ultimately helps in optimizing their response. Various factors that influence the response of polymer are its thickness, material on front and back of the polymer, area of the polymer film, and type of electrodes [1]. The open circuit voltage of a piezoelectric polymer, when a step force is applied on top is:

$$\begin{aligned}
 V_{polymer} = & -\frac{h_{zz} \times F_{in} \times (1 - R_{fp})}{Z_{ap}} \left[t - (1 + R_{pb}) \times \left(t - \frac{Z}{v} \right) \times u \left(t - \frac{Z}{v} \right) \right. \\
 & + R_{pb} \times (1 + R_{fp}) \times \left(t - \frac{2Z}{v} \right) \times u \left(t - \frac{2Z}{v} \right) \\
 & - R_{fb} \times R_{pb} \times (1 + R_{pb}) \\
 & \left. \times \left(t - \frac{3Z}{v} \right) \times u \left(t - \frac{3Z}{v} \right) + \dots \right] \tag{B.30}
 \end{aligned}$$

where, $R_{fp} = (Z_p - Z_f)/(Z_p + Z_f)$ represent the reflection coefficient at front-polymer interface and $R_{pb} = (Z_p - Z_b)/(Z_p + Z_b)$ at polymer-back faces. Z_p , Z_f , and Z_b are the acoustic impedances of polymer, and the material on the front and back (silicon in the present case) sides respectively. Z is the thickness of the polymer, v is the wave velocity in polymer and $u(\cdot)$ is the step function. It can be noted from (7.2) that the open circuit voltage of the polymer depends on the thickness of the polymer, the reflection coefficients at the two faces, internal parameters

Fig. B.12 Simulated open circuit voltage of 25, 50 and 100 μm thick polymer film. A step force of 0.1 N was applied



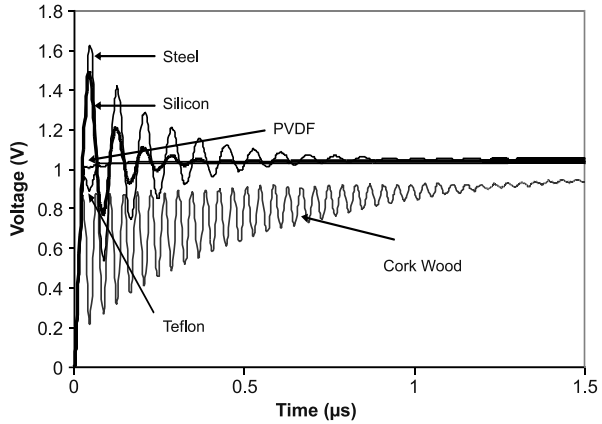
like piezoelectric constant and elastic constant (acoustic impedance). In addition to these, the capacitance of polymer is also involved when the polymer is connected with a load.

In (B.30), the term outside brackets represents the net mechanical to electrical conversion and the terms inside the bracket are combination of incident and reflected force waves. It can be observed from the first term inside brackets that the voltage is a ramp function. If the thickness of the polymer is increased, the step function terms are further delayed (delay time increases as Z is increased). Thus the open circuit voltage keeps on increasing linearly until first delay term contributes to the net voltage. Thus, the open circuit voltage in general increases with the thickness of the polymer film. This thickness effect of polymer film can also be noted from the simulation result shown in Fig. B.12. Apart from above discussed factors, the response of polymer also depends on its area, which depends on sensor configuration.

The internal properties like piezoelectric constant depend on the way the polymer is made. Uniform thin films of piezoelectric polymers like P(VDF-TrFE), can be obtained by spin coating the polymer solution and annealing it at around 100° [16]. In order to have piezoelectric properties, the piezoelectric polymer needs to be poled at a rate of (~ 100 V/ μm). The intrinsic properties of polymers depend on the way the films are processed.

The materials on the front and back of the polymer offer different acoustic impedances to the force waves. The response of polymer with different materials under polymer, simulated with the SPICE model, is shown in Fig. B.13. It can be noticed that the polymer has higher sensitivity when a stiff material is used on the back side. For stiffer materials, the reflection coefficient R_{pb} is high and the device operates in $\lambda/4$ mode. For piezoelectric polymer based sensors realized on silicon wafers, the back side is made of silicon whose acoustic impedance is approximately five times that of P(VDF-TrFE). Thus, the reflection coefficient, R_{pb} , is 0.66. This means that piezoelectric polymer based sensors having silicon under the polymer, have high sensitivity.

Fig. B.13 Response of polymer with different backside materials. Acoustic impedance of steel, silicon, PVDF, teflon and wood are 9, 3.8, 0.8, 0.6 and 0.02 MRayl respectively. A step force of 0.01 N was applied



B.8 SPICE Netlist of Piezo-Polymer Model

* source LOSSY PIEZO POLYMER

```
E_E3(Lossy_Capacitor) 3 4 LAPLACE{I(V_V3)} = 1/(s × (C0 - C0 × tan(δe) × (s/abs(s))))
R_Acoustic_Imp_back 0 BACK Zm
T_Acoustic_Transmission_Line BACK 1 FRONT 1 LEN=lx R=0 L=Lt G=Gt
C=Ct
V_V3 4 5 DC 0 AC 0 0
V_V2 E 3 DC 0 AC 0 0
E_E2(electrical) 5 0 LAPLACE I(V_V1) = h*/s
V_V1 1 2 DC 0 AC 0 0
V_Vin S 0 DC 0Vdc AC 1Vac
R_Acoustic_Imp_Front 0 FRONT Zm
E_E1(mechanical) 2 0 LAPLACE{I(V_V2)} = h*/s
R_R 5 E 1n
```

* source PIEZO LOSSY MODEL OF PUTTMER

```
V_V1 S 0 DC 0Vdc AC 1Vac
V_V2 E 3 DC 0 AC 0 0
T_T1 Back 1 Front 1 LEN=lx R=(Lt/Q) * SQR((-1 * (s) * (s))) L=Lt G=0
C=Ct
E_E1 2 0 LAPLACE I(V_V2) = h/s
R_Acoustic_Imp_back 0 BACK Zm
X_F1 1 2 0 3 SCHEMATIC1_F1
R_Acoustic_Imp_Front 0 FRONT Zm
C_C0 0 3 C0
R_R S E 1n
.subckt SCHEMATIC1_F1 1 2 3 4
F_F1 3 4 VF_F1 h × C0
```

```
VF_F1 1 2 0V  
.ends SCHEMATIC1_F1
```

B.9 Summary

The SPICE model for piezoelectric polymers presented in this chapter, for the first time, incorporates all losses namely: viscoelastic, piezoelectric and dielectric. It has been shown that, the model provides a good match between simulated and measured data and that the past approaches, developed mainly for piezoceramics, are not suitable for piezoelectric polymers. By comparing the contribution of various losses in the model, the viscoelastic losses have been found to have a major role. Perhaps, this is one reason why past approaches tried to model the viscoelastic losses only. The discussion on design issues associated with piezoelectric polymers, when they are used as transducer, provide good insight into their behavior under various conditions. Around low frequencies (~ 1 kHz), such a model can be approximated with a capacitor in series with a voltage source, as discussed in following chapters. Thus, the model presented in this chapter can be used to evaluate the performance of POSFET based tactile sensing devices, discussed in Chaps. 7 and 8, over a wide range of frequencies and can be used to explore the utility of such devices to applications other than tactile sensing as well. The successful implementation of the transducer model in SPICE, has made it convenient to evaluate the performance of transducer, both, in time and frequency domains. This implementation will greatly help in designing and evaluating the sensor system i.e., transducer and conditioning electronics, all together.

References

1. L.F. Brown, Design consideration for piezoelectric polymer ultrasound transducers. *IEEE Trans. Ultrason. Ferroelectr. Freq. Control* **47**, 1377–1396 (2000)
2. M. Redwood, Transient performance of piezoelectric transducers. *J. Acoust. Soc. Am.* **33**, 527–536 (1961)
3. S.A. Morris, C.G. Hutchens, Implementation of Mason's model on circuit analysis programs. *IEEE Trans. Ultrason. Ferroelectr. Freq. Control* **33**, 295–298 (1986)
4. W.M. Leach, Controlled-source analogous circuits and SPICE models for piezoelectric transducers. *IEEE Trans. Ultrason. Ferroelectr. Freq. Control* **41**, 60–66 (1994)
5. A. Püttner, P. Hauptmann, R. Lucklum, O. Krause, B. Henning, SPICE models for lossy piezoceramics transducers. *IEEE Trans. Ultrason. Ferroelectr. Freq. Control* **44**, 60–66 (1997)
6. R.S. Dahiya, M. Valle, L. Lorenzelli, SPICE model of lossy piezoelectric polymers. *IEEE Trans. Ultrason. Ferroelectr. Freq. Control* **56**(2), 387–396 (2009)
7. ANSI/IEEE, IEEE standard on piezoelectricity. *IEEE Standard 176-1987* (1987)
8. H. Ohigashi, Electromechanical properties of polarized polyvinylidene fluoride films as studied by the piezoelectric resonance method. *J. Appl. Phys.* **47**, 949–955 (1976)
9. K.W. Kwok, H.L.W. Chan, C.L. Choy, Evaluation of the material parameters of piezoelectric materials by various methods. *IEEE Trans. Ultrason. Ferroelectr. Freq. Control* **44**, 733–742 (1997)

10. J. Wu, G. Du, Analogy between the one-dimensional acoustic waveguide and the electrical transmission line for cases with loss. *J. Acoust. Soc. Am.* **100**, 3973–3975 (1996)
11. A.M. Vinogradov, V.H. Schmidt, G.F. Tuthill, G.W. Bohannon, Damping and electromechanical energy losses in the piezoelectric polymer PVDF. *Mech. Mater.* **36**, 1007–1016 (2004)
12. J.G. Smits, Iterative method for accurate determination of the real and imaginary parts of the materials coefficients of piezoelectric ceramics. *IEEE Trans. Sonics Ultrason.* **SU-23**, 393–402 (1976)
13. S. Sherrit, H.D. Wiederick, B.K. Mukherjee, Non-iterative evaluation of the real and imaginary material constants of piezoelectric resonators. *Ferroelectrics* **134**, 111–119 (1992)
14. TASI Technical Software Inc. Ontario, Canada (2007). Available at: <http://www.tasitechnical.com/>
15. G. Hayward, M.N. Jackson, Discrete-time modeling of the thickness mode piezoelectric transducer. *IEEE Trans. Sonics Ultrason.* **SU-31**(3), 137–166 (1984)
16. R.S. Dahiya, M. Valle, G. Metta, L. Lorenzelli, S. Pedrotti, Deposition processing and characterization of PVDF-TrFE thin films for sensing applications, in *IEEE Sensors: The 7th International Conference on Sensors*, Lecce, Italy (2008), pp. 490–493

Appendix C

Design of Charge/Voltage Amplifiers

Abstract The designs of three stage charge and voltage amplifiers, to read the taxels on piezoelectric polymer—MEA based tactile sensing chip, are presented here. Piezoelectric polymers is approximately represented as a voltage source in series with the static capacitance of the polymer. Due to the presence of capacitance, piezoelectric polymers have very high output impedance. Thus, to measure the charge/voltage generated due to applied forces, an amplifier with very high input impedance (e.g. CMOS input based) is required.

C.1 Charge Amplifier

The independence of amplifier output from the cable capacitances and the minimization of the charge leakage through the stray capacitance around the sensor, make charge amplifier a preferred choice especially when long connecting cables are present. The schematic of the charge amplifier is given in Fig. C.1. The amplifier consists of three stages. The differential charge amplifier in the first stage is followed by differential to single ended amplifier, which is then followed by a second order Sallen–Key low pass filter and a low pass RC filter. In the first stage FET input based OPA627 operational amplifiers are used. These are low noise op-amps with typical input bias current of 2 pA. In the second and third stage TL082 op-amp is used. The gain of second stage is 5 and that of third stage is 4. Overall gain of the amplifier is set by value of feedback capacitances in the first stage with respect to the static polymer capacitance. The circuit has been designed to have a frequency range of 2 Hz–200 kHz.

C.2 Voltage Amplifier

The voltage amplifiers are preferred if the ambient temperature variation is high, since they exhibit less temperature dependence and hence useful for measuring the piezoelectric polymer film response. This is due to the fact that piezoelectric polymer's voltage sensitivity (g -constant) variation over temperature is smaller than the charge sensitivity (d -constant) variation. The schematic of voltage amplifier is

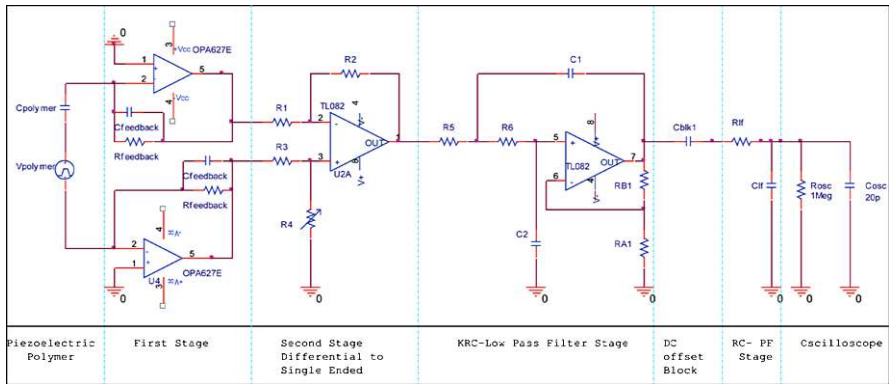


Fig. C.1 Schematic of three stage charge amplifier

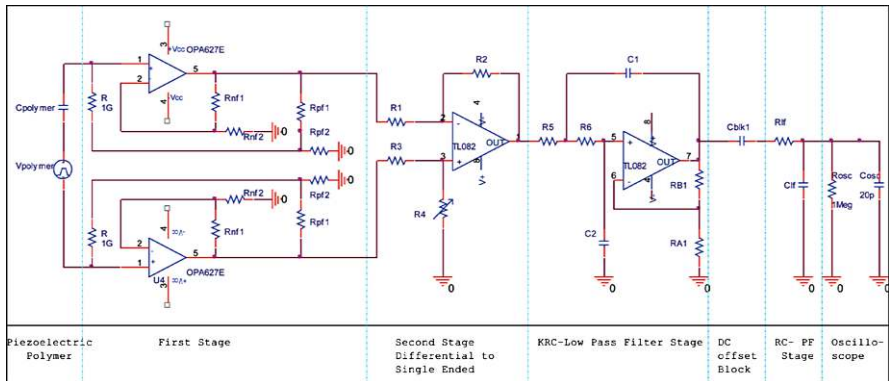


Fig. C.2 Schematic of three stage voltage amplifier

shown in Fig. C.2. It also comprises of three stages. Except first stage, remaining two stages are same as that of the charge amplifier. Since the source capacitance in the present case is ~ 1 pF, the low frequency response can be brought down to ~ 5 Hz by keeping the circuit loading effect as minimum as possible. This was obtained by providing a resistive load of 1 G Ω in the first stage. This value appears 3–5 times higher to the polymer, due to the bootstrapping technique adopted by using positive feedback. Use of resistors with resistances more than 1 G Ω is not recommended as higher values are prone to noise due to humidity, dust, temperature variation etc. With the adoption of this technique the voltage amplifier has a gain of 46 dB in the frequency range of 8 Hz–200 kHz.

Index

A

Absolute capacitance, 86
Acceleration, 126
Accelerometer, 196
Access time, 58–60, 62
Accuracy, 24
Acoustic impedance, 96, 156, 219, 223, 227, 228
Acoustic loss, 212
Acoustic transmission, 219
Acoustic wave propagation, 219
Acquisition time, 64, 190
Action for perception, 6, 15
Action potential, 22, 26, 64
Active device, 62
Active perception, 19
Active pixel, 59, 60
Active pixel sensor (APS), 59
Active taxel, 59, 60, 66
Active touch, 14, 29
Active transducer, 62
Actuator, 72, 96
Acuity, 20, 24
Adaptation rate, 22
Addressing, 58, 63, 64
Addressing scheme, 54
Algorithm, 49, 65, 67–70, 73
Algorithms, 11
Amorphous silicon, 118
Amplification, 65, 113
Amplifier, 35, 60, 63, 117, 171, 233
Amplitude modulation, 86
Analog filter, 54
Analog resistive sensing technology, 82
Analog resistive touch sensing, 81–83
Analog sensors frontend, 118
Analog to digital (A/D), 26, 60–64, 66, 71, 124

Anisotropic, 200
Annealing, 163, 164, 228
Anthropomorphic, 83, 98
Anti-aliasing, 63
Anticipatory control, 30, 31
Application specific integrated circuit (ASIC), 71
Artificial brain map, 69
Artificial intelligence (AI), 70
Artificial limbs, 3, 10
Aspect ratio, 159, 188, 190
Assistive robots, 80
Attention, 26
Audio, 25, 31, 71
Autonomous learning, 80
Autonomous robot, 61

B

Band gap, 110
Band pass filter, 63
Bandwidth, 52, 58–60, 64, 67, 68, 97, 117, 155
Barrier width, 111
Bayes tree, 69
Behavioral modeling, 219
Bendable, 47
Bendable POSFET, 191
Bendable tactile sensing chip, 191
Biasing, 61, 62, 190
Bio-robots, 80
Biomedical, 9
Biomedical robotics, 9
Biometric, 50
Bit rate (BR), 64
Body schema, 30, 31
Bootstrapping, 234
Bottom-up method, 192

C

Calibration, 65
 CAN, 67, 68, 71, 105
 Cantilever, 112
 Capacitance, 86, 104, 147, 211, 215
 Capacitance to digital converter, 89
 Capacitance-to-digital converter, 125
 Capacitive, 16, 54, 57, 58, 60, 62, 63, 81, 85–87, 89, 99, 112
 Capacitor, 85, 198
 Carbon black, 102, 106, 129
 Carbon black nanoparticle filler, 103
 Carbon fiber, 102
 Carbon microcoil filler, 103
 Carbon microcoils (CMCs), 104
 Carbon nano tube (CNT), 51, 129
 Carbon nanotube (CNT), 103
 Carbon nanotubes (CNT), 106, 107
 Carrier frequency, 64
 CCD, 91, 111
 Cellular rubber, 105
 Central nervous system (CNS), 13, 15, 26, 27, 36
 Cerebral cortex, 26
 Channel current, 120, 122
 Channel length, 160, 162, 190
 Channel width, 160, 162, 190
 Charge amplifier, 146, 147, 233, 234
 Charge carrier mobility, 122, 162
 Charge coupled device (CCD), 54, 73
 Charge neutrality, 154
 Charge sensitivity, 233
 Chip-on-flex, 191
 Chirping, 93
 Classification, 15, 151
 CMOS, 8, 91, 161, 188, 190, 191
 Coercive field, 157
 Cognition, 25, 63, 69
 Common-source, 158, 171, 173, 189, 193
 Communication, 66, 187
 Communication bandwidth, 64
 Communication bus, 66–68, 71, 124
 Communication interface, 73, 126
 Communication port, 125
 Compass method, 24
 Compensation, 65
 Complementary metal oxide semiconductor (CMOS), 59, 60, 66, 233
 Compliance, 5, 6, 8, 16, 29, 35, 49
 Compliance coefficient, 203
 Composite, 104–106
 Computational intelligence, 69, 151
 Computer aided design (CAD), 48, 74
 Computer aided engineering (CAE), 74

Computing power, 74
 Conductance, 215
 Conductive elastomer, 83
 Conductive epoxy, 114
 Conductive fiber, 83, 103, 108
 Conductive filler, 102
 Conductive fluid, 109
 Conductive gel, 83, 101
 Conductive graphite, 105
 Conductive polymer, 83, 84
 Conductive polymer composite (CPC), 107
 Conductive polymer composites (CPC), 102, 103
 Conductive polymer nanoparticle filler, 103
 Conductive rubber, 83
 Conductive yarn, 83, 103
 Conformability, 79, 101
 Conformable, 25, 29, 35, 36, 47, 48, 53, 92, 123
 Contact force, 57, 81
 Contact location, 82
 Contact point estimation, 46
 Contact pressure, 81
 Control, 36, 44, 46
 Control bandwidth, 58, 60
 Control loop, 34, 60
 Controlled source, 211, 219, 221
 Controller, 65, 67, 74
 Corona poling, 166
 Cortical neurons, 27
 Coupling factor, 214
 Creep, 90, 105, 107, 124, 125
 Cross talk, 107
 Cross-talk, 24, 60, 143, 148, 182–184
 Curie temperature, 166, 198
 Current mirror, 190
 Current sink, 188
 Curve fitting, 216
 Cut-off frequency, 149
 Cutaneous, 5, 13–16, 19–21, 23, 24, 27, 29–31, 53
 Cutaneous perception, 14
 Cutaneous system, 13

D

Data acquisition, 59, 61, 63, 64
 Data processing, 11, 64
 Data rejection, 68
 Data representation, 69
 Data selection, 68
 Data transfer, 34, 58
 Data transmission, 53, 66, 68
 Data wire, 54
 Decimation filter, 64

- Depolarization, 163
 - Dermis, 20, 21, 32, 121
 - Design hints, 33
 - Detector, 90, 93
 - Dexterous manipulation, 7, 15, 30, 44, 46, 49
 - Diaphragm, 112, 114
 - Dielectric, 195–198, 205, 208
 - Dielectric constant, 85, 120, 154, 161, 169, 204–207, 212, 215, 217
 - Dielectric effect, 204
 - Dielectric loss, 212, 214, 216, 221, 224, 227, 230
 - Dielectric loss factor, 217
 - Dielectric permittivity, 204
 - Dielectric susceptibility, 204
 - Digital converter chip, 63
 - Digital counter, 64
 - Digital signal processing (DSP), 64, 71
 - Digital to analog (D/A), 61
 - Digitalization, 63
 - Digitization, 58
 - Diode, 116, 140, 178, 185
 - Dipole, 196, 199
 - Dipole moment, 101, 196, 198
 - Direct piezoelectric effect, 199, 203
 - Discrete resistive touch sensing, 81
 - Displays, 85
 - Distributed computing, 65
 - Distributed tactile sensing, 177
 - Dorsal column medial lemniscal pathway, 26
 - Drain, 108
 - Drain current, 122
 - Duty cycle, 86
 - Dymaxion map, 48
 - Dynamic force, 118
 - Dynamic range, 60, 97
 - Dynamic response, 96
 - Dynamic sensing, 89
- E**
- Edge detection, 29
 - Effective bit rate (EBR), 64
 - Elastic compliance, 212
 - Elastic constant, 161, 204, 215, 228
 - Elastic cover, 35, 49
 - Elastomer, 46, 129, 192
 - Elastomer matrix, 102
 - Elastoresistance, 81, 83
 - Elastoresistivity, 83
 - Electric displacement, 119, 120, 154, 204, 212–214
 - Electrical equivalent, 158, 169
 - Electrical equivalent model, 146
 - Electrical impedance tomography (EIT), 51, 84
 - Electro-optic (EO), 110
 - Electrochemical, 99
 - Electrode poling, 166, 167
 - Electroluminescence, 92, 110
 - Electroluminescent, 111
 - Electromagnetic, 93
 - Electromechanical conversion, 219
 - Electromechanical coupling constant, 214
 - Electromechanical coupling factor, 207
 - Electromechanical loss, 212, 214, 216
 - Electron beam poling, 166
 - Electron tunneling, 110
 - Electronic device, 116
 - Electronic polarization, 196
 - Electronic skin, 35, 37, 57, 192
 - Electrooptical, 92
 - Electrophoresis, 164
 - Electrorheologic effect, 98
 - Electrorheological (ER), 98
 - Electrospinning, 164
 - Embedded data processing, 62, 64–66, 71, 72
 - Embedded electronics, 74
 - Embedded system, 66
 - Embroidery, 108
 - Emitter, 90, 93
 - Encapsulation, 129
 - Encoding, 25, 26, 30
 - Endoscopy, 97
 - Energy barrier, 111
 - Energy budget, 71
 - Energy harvesting, 71, 200
 - Entropy, 109
 - Epidermis, 20, 21, 29, 32, 102, 121
 - Epoxy, 157–159
 - Equivalent circuit, 142, 216, 218
 - Equivalent model, 142
 - Etching, 163, 165, 191
 - Ethernet, 67
 - Exploration, 4–8, 14, 15, 19, 28, 36, 44–46, 80
 - Extended gate, 116–118, 120, 139, 141–143, 153, 157–159, 193
 - Extrinsic optical sensor, 90, 92
 - Extrinsic sensing, 15, 16
 - Extrinsic touch sensor, 70
 - Eye-in-hand, 8
- F**
- Fabrication, 153, 161, 163, 172, 177, 179, 191–193
 - Fabrics, 51
 - Fast adapting (FA), 22, 25, 28
 - Fatigue, 65
 - Fault tolerance, 36, 72, 73
 - Feature extraction, 19, 65, 67–69

Feedback, 68
 Feedforward, 31
 FeRAM, 119, 120, 154
 Ferroelectret, 118
 Ferroelectric, 81, 99, 157, 195, 196, 198
 Ferromagnetic, 198
 Fiber Bragg grating (FBG), 92
 Field effect transistor (FET), 62, 189
 Field effect transistors (FET), 139, 141–143
 Figure of merit, 216
 Filtering, 35, 64
 Fingerprint, 29, 32, 50
 Finite element modeling, 32, 49
 Firing rate, 28
 Firmware, 65
 Flexibility, 72, 102
 Flexible, 16, 36, 47, 48, 53
 Flexible electronics, 191
 Flexible MEMS, 114
 Flexible printed circuit board, 114, 124, 125, 129
 Flexible printed circuit board (PCB), 48, 55
 Flexible tactile sensing chip, 191
 FlexRay, 67, 68
 Floating gate, 153, 171, 180
 Force, 34, 44, 65
 Force distribution, 57
 Force perception, 30
 Force sensing, 14
 Force sensing resistors (FSR), 10, 51, 83
 Force sensors, 16
 Force/torque (F/T) sensor, 58
 Force/torque sensors, 8
 Free charge, 200, 204
 Frequency modulation, 86
 Frequency response, 58
 Friction cone, 46
 Frustrated total internal reflection, 91
 Fuel cell, 71
 Fuller map, 48
 Functional block diagram, 62
 Fuzzy sets, 70

G

Gain, 58, 182, 189
 Gain plot, 148, 172
 Gain-phase plot, 189
 Gate, 108
 Gauge factor, 113, 116
 Glabrous skin, 20, 22
 Graphite, 102
 Graphite filler, 105, 106
 Graphite nanosheet filler, 103
 Grasp, 22, 30, 31, 68

Grasp control, 15, 46
 Grasp stability, 6, 7, 30, 46, 69
 Grasping, 6–8, 10, 89

H

Half wave resonance, 217
 Half-bridge, 113
 Hall effect, 93
 Hall voltage, 94
 Haptic display, 99
 Haptic interface, 99
 Haptics, 5–7, 13–15, 31
 Hardness, 6, 29, 30, 33, 46, 69, 96, 109, 115, 118, 150, 151, 179
 Hardware, 73, 129
 Hardware requirement, 47
 HDMS, 165
 Heterogeneous integration, 115
 HEX-O-SKIN, 126
 Hierarchical functional diagram, 56
 Hierarchical structural diagram, 56
 Human machine interface, 85, 89
 Human robot interaction (HRI), 73
 Human sense of touch, 19, 20, 36, 43, 44, 58
 Human–robot interaction, 3, 6, 9, 10
 Human–robot interaction (HRI), 69, 74
 Humanoid, 3, 8, 9
 Humanoids, 80
 Humidity, 36, 107
 Hybrid resistive tactile sensing, 82, 83
 Hydrophone, 196
 Hysteresis, 36, 84, 89, 90, 94, 101, 107, 110, 114, 124, 125, 157, 167, 198

I

I²C, 67, 68
 II–VI semiconductor, 110
 Image, 60
 Image processing, 51
 Imaging, 84
 Impedance, 70
 Impedance adaptation, 63, 190
 Impedance matching, 188
 Implant, 162
 In situ poling, 166, 167
 Incipient slip, 173
 Induced channel, 155
 Inductance, 104, 215
 Inductive, 16, 68
 Information transfer, 25, 26
 Inorganic semiconductor, 140
 Input characteristics, 179
 Integral sensing unit, 153
 Integral sensor unit, 192

- Integrated circuit, 192
- Integrated circuit (IC), 66, 89, 119
- Integrated circuits, 140
- Integrated read-out, 177
- Integrated smart sensor, 166
- Integrated system, 139
- Integrated temperature sensor, 177, 178
- Intelligent routing, 54
- Intelligent textile, 103, 108
- Intelligent yarn, 108
- Interconnect, 36, 50, 53, 55, 63, 68, 116, 159, 174
- Interdigitated, 104
- Interdigitated gate, 188
- Interdigitated structure, 88
- Interface circuit, 190
- Interface electronics, 57, 58, 61–63, 65, 66, 71, 72, 129
- Interfacial space charge polarization, 196
- Interference, 93
- Intermediate ridge, 21, 24, 29, 32, 35, 121
- Intrinsic conductive polymers (ICP), 103
- Intrinsic optical sensor, 91
- Intrinsic optical tactile sensing, 92
- Intrinsic sensing, 15, 16
- Intrinsic touch sensor, 71
- Ionic polarization, 196, 197
- Ionization, 109
- IRLED, 126
- ISFET, 140

- K**
- Kinematics, 7
- Kinesthetic, 5, 13–15, 19, 20, 28–30, 34, 70
- Kinesthetic perception, 14
- Kinesthetic system, 13

- L**
- Large area skin, 92
- Large scale integration (LSI), 54
- Large-area sensors, 101
- Large-area skin, 123
- LED, 124
- Lever arm mechanism, 32
- Light coupling, 93
- Light emitting diode (LED), 90
- Light spectrum, 110
- Light touch, 20, 61
- Linear theory of piezoelectricity, 203, 212
- Linearity, 60, 63
- Linearization, 65
- Liquid crystal display (LCD), 111
- Liquid crystal (LC), 107
- Liquid crystalline (LC), 98
- Lithium polymethacrylate (LiPMA), 98
- Lithography, 162
- Load cell, 145
- Local computation, 35, 55
- Local computing, 64
- Local data processing, 66
- Local memory, 60
- Local processing, 65, 187, 192, 193
- Localization, 70
- Longitudinal, 97
- Loss factor, 217
- Loss of light, 93
- Loss tangent, 214
- Lossy capacitance, 215
- Lossy capacitor, 221
- Lossy transmission line, 215, 216, 219
- Low pass filter, 63, 101, 233
- LPCVD, 162
- LTO, 163

- M**
- Machine learning, 69, 70
- Magnetic, 16, 81, 93, 99
- Magnetic coupling, 93, 94
- Magnetic flux, 93, 94
- Magneto-electric, 16
- Magnetoelastic, 94
- Magnetoresistance, 93
- Magnetorheological (MR) effect, 99
- Magnetorheological (MR) fluids, 99
- Maintainability, 74
- Maintenance, 74
- Manipulation, 6–8, 10, 28–30, 34–36, 45, 46, 79, 80, 171
- Manufacturability, 74
- Material classification, 70
- Matrix, 83, 96, 104
- Mechanical amplifier, 32, 35
- Mechanical impedance, 170
- Mechanoreceptor, 43, 65, 161, 174
- Mechanoreceptors, 4, 20–22, 24–26, 28, 29, 34, 35
- Medical robots, 80
- Meissner's corpuscles, 20, 22
- Melting point, 193
- MEMS, 83
- Merkel cells, 20–22, 29, 32
- Metal nanoparticle filler, 103
- Metal oxide semiconductor (MOS), 153, 154, 157–161, 163, 165, 167, 169–172, 179, 188
- MFMS, 119, 154
- Micro bending, 93
- Micro tactile element, 105

Micro-/nano-structures, 35
 Micro-/nanowires, 35
 Micro-lever action, 29, 32
 Microbending, 93
 Microcontroller, 64, 67, 68, 71, 73, 105, 124, 126
 Microelectrode array (MEA), 233
 Microelectrode (MEA), 139, 141, 143–148, 151
 Microelectromechanical system (MEMS), 66, 85, 88, 89, 112–116
 Microelectronics, 54, 114
 Microfluidics, 51
 Micromachining, 97, 112, 114–116
 Microphone, 196
 Microprocessor, 55, 65
 Microstructure, 196
 Microstructures, 24
 Miniaturization, 33, 47, 72, 139, 140, 188
 Minimal invasive surgery, 6, 9
 Minimally invasive surgery, 97
 Mobile robots, 45
 Model, 219, 221, 227, 230
 Modeling, 15, 169, 211
 Modular, 36, 72, 73
 Modularity, 72
 Modulating frequency, 64
 Module, 48, 49, 53, 65, 72, 73
 Molecular model, 198
 MOS, 117, 119
 MOSFET, 117, 140, 141, 153, 155
 Motion planning, 69, 126
 Motion strategies, 4
 Motor control, 14, 19, 30
 Moving average, 64
 Multi-walled carbon nanotube (MWNT), 106
 Multifunctional, 33
 Multimodal, 57, 70, 115, 126
 Multiplexer, 63, 105
 Multiplexing, 55, 65
 Multiplexor, 190
 Mutual capacitance, 86–88

N

Nanocomposite, 106, 107
 Nanoparticle, 92, 111
 Nanoparticles, 110
 Nervous system, 65
 Network, 67
 Networking, 74
 Neural network, 69, 70
 Neural pathways, 26
 Neuromorphic, 66
 Newtonian fluid, 98

Nociceptors, 20
 Nocioceptor, 43
 Non invasive, 84
 Non linear regression, 217
 Non-polar dielectrics, 198
 Non-volatile memory, 196
 Nonferromagnetic, 99
 Nonlinear regression, 215
 Normal force, 86
 Normal strain, 112
 Normal stress, 112, 113
 Nyquist rate, 59, 60, 64

O

Object identification, 151
 Object recognition, 15, 19, 29, 49, 69, 79, 182
 Off-the-shelf, 123
 On-chip electronics, 158, 188, 189, 193
 On-chip read-out, 190
 On-chip signal conditioning, 188
 Operation amplifier, 233
 Optical, 16, 81, 90, 99, 110, 123
 Optical arrays, 191
 Optical fiber, 90, 91, 93
 Optical imager, 66
 Optical tactile sensor, 93
 Optical waveguide, 91
 Optimization, 52
 Organic field effect transistor (OFET), 58, 59, 120
 Organic semiconductor, 140
 Organic transistor, 116
 Orientation grating method, 24
 Orientation polarization, 196
 Oscillator, 64, 195
 Output buffer, 188, 190
 Oversampling, 59, 60, 64

P

Pacinian corpuscles, 20–22, 29, 32
 Packaging, 113, 129, 148, 193
 Pain, 5, 20
 Palpation, 9
 Papillary ridge, 29, 32, 35
 Paelectric, 198
 Parallel processing, 15
 Parasitic capacitance, 86
 Particle filter technique, 68
 Passivation, 143
 Passive device, 62
 Passive perception, 19
 Passive pixel, 59
 Passive touch, 14, 29
 Passive transducer, 62

- PDMS, 49, 51, 88, 89, 107, 116, 121, 171, 172, 174, 182
- PECVD, 143, 163
- Peg-in-hole, 8
- Pentacene, 120
- Perception, 14, 15, 20, 24, 25, 27–29, 31, 32, 70
- Perception for action, 6, 15
- Percolation theory, 102
- Percolation threshold, 102, 103, 106, 107
- Percolation transition, 105
- Peripheral nervous system, 14
- Permeability, 94
- Permittivity, 86, 161
- Personal digital assistants (PDA), 82
- pH, 109, 116
- Phase, 58
- Phase plot, 148, 149, 172
- Photo-semiconductor device, 140
- Photodetector, 90
- Photodiode, 91, 109
- Photolithography, 165
- Photoluminescence, 110
- Photoreceptor, 66
- Photoreflector, 92
- Piecewise linear mapping, 70
- Piezo-ignition, 196
- Piezoceramic, 211, 212, 222, 224, 230
- Piezoelectric, 16, 54, 57, 58, 64, 96, 101, 109, 120, 155, 157, 195, 196, 198–205, 207–209
- Piezoelectric constant, 97, 101, 120, 142, 149, 154, 157, 161, 165, 206, 212, 215, 217, 219, 228
- Piezoelectric effect, 101, 165, 195, 196, 198, 201–204
- Piezoelectric loss, 219, 224, 227, 230
- Piezoelectric phenomenon, 195, 203
- Piezoelectric polarization, 204
- Piezoelectric polymer, 60, 116, 118, 119, 139, 141–143, 147, 151, 153–155, 159–161, 163, 164, 167, 179, 193, 211, 212, 214, 216, 221, 222, 227, 228, 230, 233
- Piezoelectric resonator, 217
- Piezoelectric strain coefficient, 203
- Piezoelectric stress constant, 203
- Piezoelectricity, 195, 196, 198, 203, 205, 209
- Piezoresistance, 81, 83
- Piezoresistive, 54, 83, 89, 102, 105, 108, 112, 113, 120, 124, 155
- Piezoresistive effect, 120, 172
- Pixel, 66
- Polar dielectrics, 197
- Polarization, 98, 101, 122, 154, 155, 168, 179, 180, 193, 195–200, 202–206, 208
- Polarization effect, 200
- Polarization level, 167
- Polarization phenomenon, 198
- Polarization vector, 203
- Poling, 101, 153, 161, 163, 165, 166, 201, 204, 228
- Poly(allylamine hydrochloride) (PAH), 110
- Polyaniline (PANI), 103
- Polyelectrolyte gels, 109
- Poly(ethylene naphthalate) (PEN), 120
- Polymer gels, 108
- Polymer matrix, 102, 105
- Poly(methyl methacrylate) (PMMA), 105
- Polypyrrole (PPy), 103
- Polysilicon, 84, 112, 116
- Polystyrene (PS), 105
- Poly(styrene sulfonate) (PSS), 110
- Poly[styrene-*b*-(ethylene-cobutylene)-*b*-styrene] (SEBS), 106
- Polythiophene (PTh), 103
- Polyurethane (PU), 107
- Portability, 72
- Portable, 36
- Pose, 52
- POSFET, 64, 66, 98, 116, 119, 151, 153–174, 177–185, 187–193, 196, 230
- POSFET array, 189, 190
- POSFET tactile sensing chip, 177
- POSPET, 155
- Potentiometer, 81
- Power consumption, 60, 62, 71, 74, 97
- Power management, 71
- Power supply, 71, 72
- Pre-processing, 15, 26, 65
- Precise manipulation, 44, 177
- Precision, 9
- Precision grip, 31
- Prehensile, 30
- Pressure, 20, 44
- Pressure conductive rubber, 58–60, 84, 120, 121
- Pressure sensitive elastomer, 106
- Pressure sensitive ink, 83, 101
- Pressure sensitive rubber, 122
- Pressure sensor, 125, 140, 172
- Pressure sensor array, 106
- Pressure threshold, 25, 51, 178
- Primary afferent fibers, 27
- Printed circuit board (PCB), 48, 94, 105, 112, 123, 126, 146
- Printing electronics, 191

- Programming tool, 53
 Programming tools, 48
 Propagation delay, 119
 Proprioception, 5, 26, 31, 46, 70
 Proprioceptor, 20
 Prosthetics, 9, 10, 110
 Proximity, 57, 89, 126
 Proximity sensing, 46
 Proximity sensor, 126
 Proximity sensors, 45
 PSPICE, 170, 218, 219, 221, 222
 Pulse width modulation, 124
 Pulse-echo method, 221
 PVDF, 57, 58, 95, 97, 102, 117, 119, 139, 141, 142, 154, 156, 157, 166, 170, 196, 198, 201, 206, 208, 212, 216, 217, 222–224
 PVDF-TrFE, 118, 120
 P(VDF-TrFE), 139, 141, 142, 144, 148, 153–157, 163–166, 170, 172, 173, 187, 189, 193, 198, 201, 207–209, 217, 222–224, 228
 Pyroelectric, 57, 98, 155, 157, 173, 187
 PZT, 96, 102, 154, 155, 198, 217
- Q**
- Quality factor, 224
 Quantum size effect, 110
 Quantum tunneling, 103
 Quantum tunneling composites (QTC), 85, 103
- R**
- Ramp function, 228
 Re-configure, 73
 Reaching, 30
 Read out, 62, 64, 115
 Read-out, 190, 193
 Real-time communication, 124
 Receptive field, 15, 16, 22–24, 27, 28, 69
 Redundancy, 72, 73
 Redundant data, 187
 Reflection coefficient, 227, 228
 Refractive index, 91, 110
 Rehabilitation, 9, 10, 80, 99
 Relaxation oscillator, 86
 Relaxation time, 62, 122
 Reliability, 43, 67, 68, 72, 73, 159
 Remanent polarization, 119, 154, 157, 163, 166, 169, 202
 Repeatability, 9, 36, 114
 Reproducibility, 117
 Resistance, 104, 215
 Resistive, 16, 62, 81, 99
 Resistive sensors, 81
 Resistive tactile sensing, 85
 Resistive tactile sensors, 81
 Resolution, 82, 85, 89, 92, 93, 96, 98, 106, 111, 116, 173
 Resonance, 225
 Resonant frequency, 68, 86, 96, 151
 Resonator, 195
 Response, 44, 45
 Response speed, 82
 Response time, 58–60
 Reverse piezoelectric effect, 200, 203
 Rheological, 99
 Robot interaction, 8
 Robot skin, 70
 Robot-assisted touch therapy, 10
 Robotic skin, 6
 Robotic surgery, 9
 Robotic tactile sensing, 192
 Robots in education, 11
 Robustness, 74
 Rolling, 185
 Roughness, 29, 31, 115
 Roughness perception, 30
 Routing, 49, 53, 54, 73, 115
 Row-column scanning, 59
 Row-column scheme, 54
 Ruffini corpuscles, 20–22
- S**
- Safe grasp, 69
 Safe interaction, 44, 126
 Sallen key low pass filter, 233
 Sampling rate, 64
 Sampling time, 58
 Sawyer tower circuit, 167
 Scalability, 72, 88, 116
 Scalable, 36, 92, 123
 Scanning rate, 58–60
 Scanning time, 59, 83
 Second order neurons, 27
 Self capacitance, 86, 87
 Self diagnostics, 74
 Self healing, 74
 Self-assembly, 110
 Self-organizing map (SOM), 69
 Semiconductive yarn, 108
 Semiconductive yarns topology, 108
 Semiconductor, 142, 162
 Semiconductor device, 139, 140
 Semiconductor nanocrystals, 110
 Semiconductor sensor, 140
 Sense of touch, 3–6, 8, 13, 14, 31, 43, 159
 Sensitive, 155
 Sensitive skin, 80, 85

- Sensitivity, 20, 24, 25, 28, 29, 32, 34, 51, 60, 86, 88, 92, 94, 97, 100, 102, 104–107, 110, 116, 119, 120, 122, 124, 145, 178, 187, 189, 193
 - Sensor, 72
 - Sensor distribution, 51
 - Sensor fusion, 19, 67–70, 129
 - Sensor hardware, 47
 - Sensor integration, 139, 140
 - Sensor placement, 47, 51, 52
 - Serial access, 60
 - Serial bus, 68
 - Service robot, 70
 - Shannon's theorem, 58
 - Shape, 5, 6, 27–31, 34, 44, 69
 - Shear, 97
 - Shear force, 46, 91
 - Shear strain, 112
 - Shear stress, 112, 113
 - Sigma-Delta modulation, 86
 - Signal conditioning, 55, 58, 61–66, 115, 126, 188
 - Signal processing, 115, 116, 139, 159
 - Signal-to-noise ratio (SNR), 59, 97
 - Signal-to-noise (S/N) ratio, 116
 - Silicon micromachining, 112, 113
 - Silicon on insulator (SOI), 191
 - Silicon technology, 88
 - Silicone matrix, 103, 104
 - Simulation, 169, 221
 - Simultaneous localization and mapping (SLAM), 70
 - Size, 69
 - Size perception, 31
 - Skin, 20, 25, 27–30, 32, 34, 35, 54, 55, 65, 68, 89, 101, 109, 115, 116, 120, 123, 124
 - Skin area, 55
 - Skin elasticity, 34
 - Skin mechanics, 29, 32, 35
 - Skin stiffness, 32
 - Skin surface area, 32, 35
 - Skin thickness, 32, 35, 55, 192
 - Skin weight, 32, 35, 47, 55, 192
 - Slip, 29, 30, 46, 65, 95
 - Slow adapting (SA), 22, 25, 28, 29
 - Small signal equivalent, 158
 - Smart fabrics, 66
 - Smart material, 96, 139, 141, 155, 173
 - Smart textile, 108
 - Smart vision, 66
 - Social robots, 80
 - Soft touch, 126
 - Soft-touch, 45, 46
 - Softness, 6, 29, 70, 96, 109, 110
 - Software, 73
 - Solid state optical sensor, 91
 - Somatosensory cortex, 15
 - Somatosensory system, 27, 43, 69
 - Somatotopic alphabet, 69
 - Somatotopic map, 26, 27, 35, 69, 70
 - Sonar, 196
 - Source, 108
 - Source-follower, 160, 171, 173, 180, 189, 193
 - Spatial acuity, 21, 24, 177, 178
 - Spatial filtering, 49
 - Spatial resolution, 16, 24, 32–34, 50, 51, 60, 92, 105, 111, 112, 116–118, 124, 125, 129, 143, 148, 155, 159, 177, 178, 182, 184, 190, 193
 - Spatio-temporal, 28, 51, 73, 151, 178
 - SPICE, 211, 212, 218, 219, 221–224, 226, 228–230
 - Spike, 26
 - Spin-coating, 164
 - Spinal cord, 26
 - Spinothalamic pathway, 26
 - Spontaneous polarization, 165, 198
 - Stability, 117
 - Step function, 227, 228
 - Stiffness, 6, 9, 16, 32, 46, 95, 100, 112, 155, 203
 - Strain, 57, 203
 - Strain gauge, 98, 115, 116
 - Strain sensor, 104
 - Stress, 57, 119, 203
 - Stress rate, 57
 - Stress/strain, 107
 - Stretchability, 50, 129
 - Stretchable, 36, 47, 84
 - Stretchable skin, 51
 - Substrate capacitance, 158
 - Super resolution algorithm, 51
 - Surface charge density, 205
 - Surface parametrization, 70
 - Synapse, 36
 - Synthetic polymer, 156
 - System architecture, 63
 - System in package (SIP), 66, 193
 - System on chip (SOC), 66, 177, 188, 191, 193
- T**
- Tactile, 33, 70
 - Tactile actuator, 99
 - Tactile acuity, 24, 159
 - Tactile classification, 14
 - Tactile fabric, 47
 - Tactile image, 7, 51
 - Tactile imaging, 85

- Tactile perception, 14, 110
 - Tactile representation, 26, 27, 30, 34, 35
 - Tactile sensing, 3, 4, 6, 9–11, 14–16, 19, 20, 28, 30, 45, 58, 79, 80, 99, 107, 122, 140, 230
 - Tactile sensing array, 15, 16, 58, 64, 88, 98, 107, 116–118, 123, 139–141, 143, 148, 151, 178, 188, 189, 192, 193
 - Tactile sensing arrays, 79
 - Tactile sensing chip, 139, 141, 145, 147, 177–182, 184–187, 189–191, 193, 233
 - Tactile sensing structure, 112, 113, 116, 120, 123, 129, 188, 191
 - Tactile sensing system, 43, 44, 46, 47, 56, 63, 65, 68, 69, 72–74, 105, 191
 - Tactile sensing system on chip, 188, 191
 - Tactile sensing technologies, 80
 - Tactile sensitivity, 50
 - Tactile sensor, 15, 16, 19, 24–26, 30, 33–37, 44, 46, 57, 58, 62, 69, 74, 79, 80, 83–86, 89, 93, 96, 97, 104, 105, 110, 114–117, 140, 142
 - Tactile sensor array, 33, 57, 61, 66
 - Tactile sensor sheet, 124
 - Tactile sensor technology, 129
 - Tactile sensor types, 45
 - Tactile sensors, 9, 85
 - Tactile skin, 35, 48, 50, 55
 - Tactual perception, 14
 - Tangential force, 86
 - Task classification, 45
 - Taxel, 52, 70, 140, 142, 143, 145–151, 171, 193
 - Technology spread, 62, 179
 - Telegraphist's equations, 215
 - Telemedicine, 9
 - Teleoperation, 9
 - Temperature, 5, 6, 15, 20, 25, 26, 36, 44, 45, 57, 65, 70, 107, 116, 126, 140, 165
 - Temperature diode, 178, 185–187
 - Temporal acuity, 25
 - Tensor, 97
 - Textile technologies, 108
 - Texture, 5, 6, 8, 14, 24, 29, 30, 32, 34, 35, 65, 69, 70
 - Thermal, 33
 - Thermal conductivity, 115
 - Thermal poling, 166
 - Thermal resistor, 115
 - Thermoeceptors, 20
 - Thermoreceptor, 43
 - Thin film transistor (TFT), 118, 192
 - Threshold voltage, 140, 141, 179
 - Time constant, 159
 - Time delay, 219
 - Time multiplexing, 62, 63
 - Top-down, 47
 - Top-down method, 192
 - Total internal reflection, 91
 - Touch receptor, 109
 - Touch screen, 82
 - Touch sensing, 15
 - Touch sensing device, 153, 159
 - Touch sensor, 7, 84, 109, 140, 141, 154
 - Traction sensors array, 112
 - Traction stress, 113
 - Trade-off, 74, 159, 160
 - Transducer, 192
 - Transconductance, 159, 179, 188
 - Transduce, 57
 - Transducer, 56, 58–60, 62, 65, 66, 72, 116, 117, 122, 126, 139, 140, 151, 153, 157, 174, 195, 211, 219, 222, 230
 - Transducer bandwidth, 58, 59
 - Transduction, 25, 34, 54, 57, 58, 60, 65, 79–81, 99, 112
 - Transformation, 51
 - Transformer, 170, 219
 - Transistor, 112, 116, 118, 120, 122, 141–143, 153, 157–162, 167, 171, 174, 192
 - Transmission, 25, 66, 68
 - Transmission line, 169, 170, 212, 215, 219, 223, 224
 - Transmission loss, 224, 227
 - Transversal, 97
 - Triangulation, 48
 - Trigeminal somatic sensory system, 26
 - Tuned resonator, 68
 - Tunneling effect, 106
 - Two points threshold, 24, 33, 34
- U**
- Ultrasonic, 16, 70, 81, 95, 99, 142, 196
 - Ultrasonic receiver, 95
 - Ultrasonic transmitter, 95
 - Unstructured environment, 6, 8, 10, 45, 46
- V**
- Very large scale integration (VLSI), 66
 - Vibration, 20, 24, 26, 44, 70
 - Vibrotactile, 5, 24
 - Viscoelastic, 26, 32, 110, 219
 - Viscoelastic loss, 211, 214, 216, 217, 230
 - Visible light, 110
 - Vision, 25, 31, 49, 70, 71, 79
 - Vision camera, 69
 - Vision imager, 60
 - Voltage amplifier, 146, 233

Voltage divider, 113
Voltage sensitivity, 233
Vulcanized liquid silicone rubber, 106

W
Wave propagation, 212
Wavefront, 96
Wavelength shift, 92
Wheatstone bridge, 113
Whole body sensing, 45, 47, 48, 54, 69, 79, 80
Wireless communication, 53, 68
Wireless transmission, 68

Wiring, 44, 74
Wiring complexity, 52–54, 63, 66, 68, 73, 116,
151, 193
Workability, 102
World model, 68

Y
Young's modulus, 32, 113

Z
ZnO, 101